DETERMINING CRITICAL NOTCH SIZE IN MISSILE LAUNCH TUBE FRONT COVER FOR SEPARATION IN SPECIFIED DIRECTION

FÜZE FIRLATMA TÜPÜ ÖN KAPAĞINDA BELİRLENEN YÖNDE AYIRMA İÇİN KRİTİK ÇENTİK BOYUTUNUN BELİRLENMESİ

HASAN ÇİÇEK

PROF. DR. BORA YILDIRIM

Supervisor

Submitted to

Graduate School of Science and Engineering of Hacettepe University

as a Partial Fulfillment to the Requirements

for the Award of the Degree of Master of Science

in Mechanical Engineering

2023

I dedicate this work to my dear son, my great wife and my family who brought me to this day.

ABSTRACT

DETERMINING CRITICAL NOTCH SIZE FOR IN MISSILE LAUNCH TUBE FRONT COVER FOR SEPARATION IN SPECIFIED DIRECTION

Hasan CICEK

Under a specific loading condition, the canister front cover must fracture in a predetermined direction upon impact from the missile radome. To prevent the broken pieces from come into contact with on the missile body, wing or tail again, the fragments should move away from the missile trajectory. In addition, a crucial consideration in the design of the canister front cover is ensuring that the load transferred from the missile radome to the seeker after the collision is less than the load it will experience during mission execution.

This thesis investigates the loads acting on the front cover of the canister and outlines the design steps taken to address them. A material characterization study was conducted on the foam material employed in the cover's production. The outcomes of this study were employed to establish the essential material library for finite element analysis. The

dimensions of the notches present on the canister front cover, which cause stress concentration, were identified via explicit analyses. Subsequently, canister front covers, produced according to the notch dimensions determined, were successfully tested in a test setup.

ÖZET

FÜZE FIRLATMA TÜPÜ ÖN KAPAĞINDA BELİRLENEN YÖNDE AYIRMA İÇİN KRİTİK ÇENTİK BOYUTUNUN BELİRLENMESİ

Hasan ÇİÇEK

Yüksek Lisans, Makine Mühendisliği Bölümü

Tez Danışmanı: Prof. Dr. Bora YILDIRIM

Nisan 2023, 81 sayfa

Belirli yük koşulu ile önceden belirlenmiş doğrultuda, füze radomunun çarpması sonucunda kanister ön kapağın kırılırak açılması gerekmektedir. Kırılan parçaların tekrar füze gövdesine, kanat veya kuyruğuna temas etmemesi için füze yörüngesinden uzaklaşmalıdır. Tüm bunlara ek olarak, kanister ön kapak tasarımında en önemli parametre çarpışma sonrasında füze radomundan arayıcı başlığa aktarılan yükün, görev icrasında maruz kalacağı yükten az olmasıdır.

Tez kapsamında tasarım basamakları açıklanan kanister ön kapağa etki eden yükler belirlenmiştir. Kapağın üretiminde kullanılan köpük malzeme için malzeme karakterizasyon çalışması yürütülmüştür. Malzeme karakterizasyon çalışması çıktıları sonlu elemanlar analizi için gerekli malzeme kütüphanesinin oluşturulmasında kullanılmıştır. Açık çözücü methodu ile gerçekleştirilen dinamik analizler ile kanister ön

kapak üzerinde yer alan ve gerilim yığılmasına sebep olan çentiklerin boyutları belirlenmiştir. Belirlenen çentik boyutlarına göre üretimi gerçekleştirilen kanister ön kapakları test düzeneğinde başarılı bir şekilde test edilmiştir.

Anahtar Kelimeler: Kırılgan Kapak, Kanister, Sabot, Açık Çözücü Methodu, Sonlu Elmanlar Methodu, Çentik

ACKNOWLEDGEMENT

To esteemed Professor Bora Yıldırım, my valuable advisor who guided me throughout my postgraduate studies, from whom I constantly benefited from his wealth of knowledge and who encouraged me in my most hopeless moments,

To Tolga Özkaya and Emel Mahmutyazıcıoğlu, who supported me without hesitation in transforming my work into a thesis,

Endless thanks...

Hasan ÇİÇEK

April 2023, Ankara

TABLE OF CONTENTS

LIST OF FIGURES

LIST OF TABLES

LIST OF SYMBOLS AND ABBREVIATONS

Symbols

A_b	Area of Burned Solid Propellant
A_t	Area of Throat
A_2	Exit Area of Nozzle
c	Wave Speed
c_e	Reference Sound of Speed in Porous Material
C_r	Surface (Rayleigh) Wave
c_s	Reference Sound of Speed in Solid Material
C_Y	Constant in Eqn [10.2]
el	Elastic Curve
f	Safety Factor
F	Thrust Force
h	Characteristic Length of Element
k	Ratio of Specific Heat
K_0	Bulk Modulus
L_{ex}	Distance Between Rocket Nozzle and Canister Front Cover
$\dot{m}$	Mass of Propellant Burned in a Unit Time
n	Compaction Exponent
R	Universal Gas Constant
P_e	Pressure Plastic Behavior of $P - \alpha$ Material Initiated
pl	Plastic Curve
P_{max}	Maximum Pressure Experienced by Material
P_s	Solid Material Pressure

p_1	Chamber Pressure
p_2	Pressure at Nozzle Exit
p_3	Ambient Pressure
r	Burning Rate
S_1	Mie Grunisen Shock Parameter
S_2	Mie Grunisen Shock Parameter
T_{max}	Maximum Temperature
Up	Velocity of Particle
Us	Velocity of Shock
V	Specific Gravity
V_{long}	Longitudinal Wave Speed
V_s	Shear Wave Speed
V_2	Exit Velocity of Exhaust Gas
α	Degree of Porosity
α_{min}	Minimum Value of α Achieved by Material
ε_x	Strain in X Direction
ε_y	Strain in Y Direction
λ	Lame's First Parameter
μ	Lame's Second Parameter
ρ	Density
$\dot{\rho}_s$	Solid Material Density
σ_h	Hydrostatic Pressure
ν	Poisson ratio
Γ	Gruneisen Parameter
∇^2	Operator in Eqn [20.2]

Abbreviations

CEA	Chemical Equilibrium and Applications
CFL	Courant-Friedrich-Levy
CNC	Computer Numerical Control
EMC	Electromagnetic Compatibility
EMI	Electromagnetic Interference
EOS	Equation of State
EQN	Equation
FEA	Finite Element Analysis
FEM	Finite Element Method
LASL	Los Alamos National Laboratory
LV	Launch Vehicle
PCB	Printable Circuit Board

1. INTRODUCTION

The system that helps to reduce the impact of the environmental conditions in which the missile will remain throughout its life cycle and to help the missile leave the launcher in a safe and stable manner is called a canister. Following the firing of the missile, the radome tip contacts the fragile canister front cover. It is aimed that the missile will break the front cover with a load lower than the load it will be exposed to in flight conditions, and the broken cover will not remain in the flight trajectory.

The load to be transferred to the missile structure with the contact of the radome tip may cause crack initiation. This crack initiation may progress in the performance of the task and result in the deterioration of the structural whole. Because; it is aimed to reduce the strength of the canister front cover with the notch, which will provide stress concentration in predefined areas and where it will be divided into parts. So that missile will achieve to break canister front cover with the load less than the load to which will be exposed during the flight. On other hand batteries contains more than one missile. Canister covers must be resistant to the rocket exhaust plume when the adjacent missile is fired.

Because the missile has high acceleration, in other words, the jerk is also positive, the collision must be damped and cushioned. Considering this situation, the foam materials are preferred. In addition to this, because of the requirements defined in MIL-STD-810H are among the success criteria of the cover design, it is not possible to select a catalog product. In order to determine the properties of the material to be developed, explicit dynamic analyzes should be performed.

In order to verify how a foam material will perform in use, test specimens are prepared Then material characterization tests are performed with these specimens to to determine its suitability for this application. However, there are some methods for measuring the Poisson's ratio of foam materials, but there is no internationally accepted method or standard required to do so. Some common techniques include using compression or

1

tensile testing machines to measure the foam's mechanical properties and then calculating the Poisson's ratio based on the resulting data. Overall, the measurement of Poisson's ratio in foam materials is an active area of research, and various methods are used to determine this property. However, the lack of an internationally accepted standard means that different researchers may use different methods or techniques, making it challenging to compare results across different studies.

Furthermore, a thorough comprehension of the physical interactions that take place prior to the missile's ejection from the canister is crucial for effective system design and analysis. Unfortunately, there is a lack of adequate academic research on this subject available in publicly accessible sources. The loads acting on the canister cover after ignition of the missile engine were determined by collecting and filtering test data during flight test.

After establishing the material properties and analyzing the loads on the system, finite element analysis was conducted to calculate the appropriate depth and width of notches on the canister cover. This was done to reduce the force transmitted to missile seeker which is made by the glass-ceramic material upon impact between the missile nose and the canister cover.

As a result of the high cost and inherent risks associated with flight testing, it is standard practice to subject the components of missile systems to conduct verification testing of design and analysis studies undertaken during the ground-based developmental phase. The prototype covers were tested on the test stand, and the resulting data were compared and correlated with the analysis study.

2. LITERATURE SEARCH

2.1. Canister Covers

Different types of canister cover can be found during the literature search. The specifications for launch tube cover mostly stem from the purpose of usage and the conditions that it will experience throughout its service life. Although they differ in material and working principle, the canister covers can be examined in 5 different groups

- Electromechanical Driven Covers
- Mechanism Activated Covers
- Canister Covers Ruptured by Blast Effect
- Covers Broken by Radome Impact
- Pyrotechnic Containing Canister Covers

2.1.1. Electromechanical Driven Covers

Ball screws powered by electric motors rely on contact switches to indicate open and closed positions. The ignition sequence is not initiated until multiple feedbacks confirm the cover is safely open to prevent accidents and enhance reliability.

The canister cover, which is opened just before the ignition sequence, is kept fixed while in the open position by a brake system on the electric motor. This braking system prevents the cover of the canister from being closed by the plum load acting on the cover while the missile leaves the canister.

When the cover is opened, it becomes vulnerable to environmental effects. To minimize this impact, the cover must be opened close to the ignition sequence. Having a fast-opening speed for the cover is very important, and that's why some systems use gear reducers in conjunction with the electric motor to decrease the time it takes to open. If the canister needs to be sealed, the front cover can be sealed with the assistance of the electric motor and gear reducer. The electric motor exerts pressure on the sealing element by pulling the cover.

These systems often have self-locking mechanisms. Hsiung Feng III developed by the National Chung-Shan Institute of Science and Technology was an example of electromechanical driven canister covers is given in Figure 1.
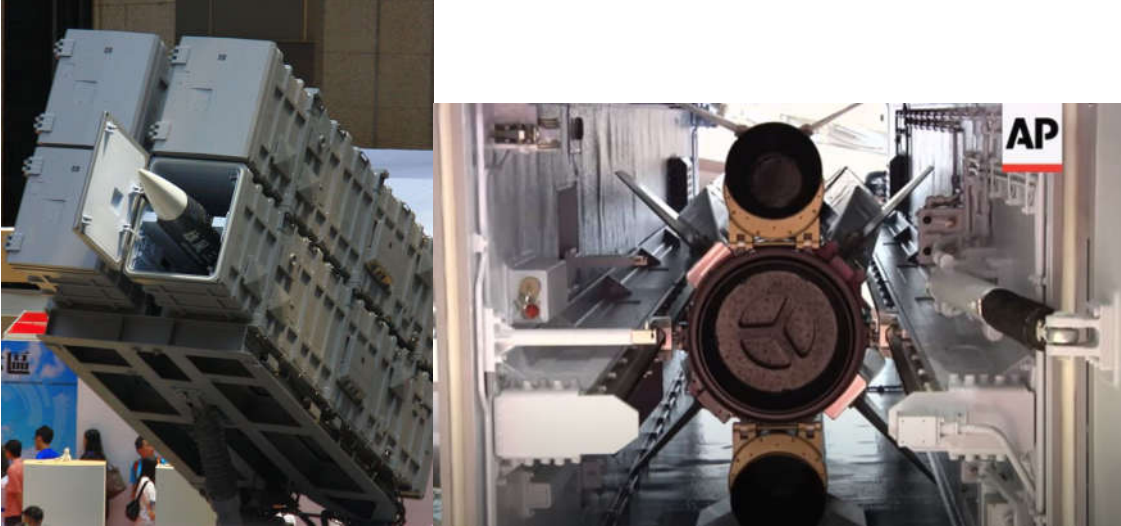
Figure 1 Hsiung Feng III Electromechanical Driven Canister Cover [1]

In addition, there are internationally patented systems in electromechanical driven cover applications. A schematic view of patents encountered during literature search is seen in Figure 2.
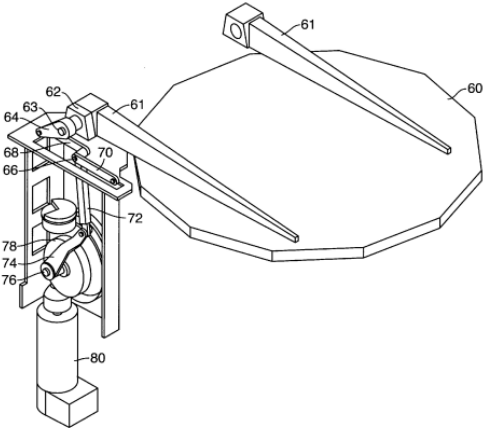
Figure 2 Electromechanical Driven Canister Cover Example [2]

It is preferable that the information on how many ammunitions is left in the system cannot be observed by the enemy elements. For this reason, the fact that the canister covers can be closed again after the performance of the task provides a tactical advantage. Many sub-parts of this system are in the commercial off-the-shell category. In other words, it is designed, tested and ready to use by original equipment manufacturer companies.

On the other hand, electromechanical systems reduce system reliability due to the complexity of the system. Failure to perform the operation in the event of a possible malfunction is considered as one of its disadvantages. Extra precautions must be taken so that the system can pass the ground verification tests and complete its life cycle.

2.1.2. Mechanism Activated Covers

They are the systems that open mechanically driven by the missile motion within the canister and then close again when the missile leaves the canister. The canister cover of the Naval Strike Missile, produced by Kongsberg Defense & Aerospace company and still in service, is driven by this principle. The visual of the related system is given in Figure 3.

Figure 3 Naval Strike Missile, Produced by Kongsberg Defense & Aerospace [3]

Before the missile is fired, information should be created whether the cover has been opened or not. In mechanism driven systems, if the drive link is broken at any point, the part carrying the missile avionics and warhead will collide with the metal canister cover. This could lead to catastrophic outcomes. It has a higher weight compared to other

alternative systems due to the large number of subcomponents. They are not preferred in most military applications due to their compelling weight budget.

However, the absence of sensors in the system exposed to environmental effects and the low complexity of the system can be listed as advantages. Moreover, for large caliber launch canisters, the front cover will be significantly heavy and could potentially cause significant damage to ground equipment.
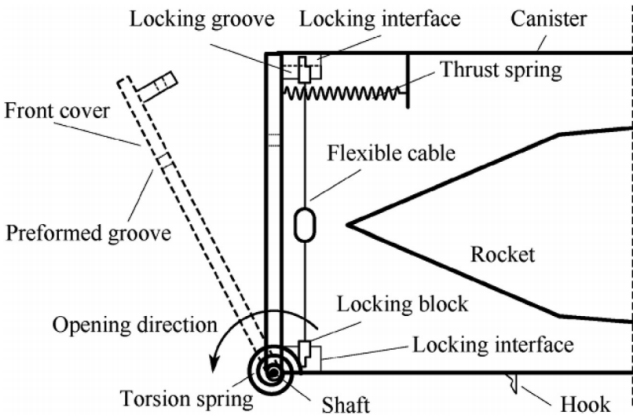
Figure 4 Schematic View of Mechanically Driven Canister Cover [4]

2.1.3. Canister Covers Ruptured by Blast Effect

It is preferred in systems where the missile radome is likely to be damaged during contact. It is expected that the cover will break or rupture with the instantaneous pressure wave that occurs during the firing of the missile engine. The shock wave that reaches the front cover by being damped in the canister causes the cover to break or rupture. During this time, the required distance for the contact of the missile radome with the cover could not be traveled.

Ruptured parts remaining in the missile trajectory may damage the missile coating and stick to the wing or tail, directly affects the dynamics of the missile. They usually have notches that increase strain concentration so that rupture can occur following this area.

Thus, ruptured pieces are move away in a predetermined path. The parts moving away from the missile trajectory will be less likely to interact with the missile structure.

The extent to which the dynamic pressure wave is can be determined by internal ballistics analysis or by dynamic pressure gauges placed near the cover during development tests. Although this dynamic pressure can be measured with sensors or determined by internal ballistic analysis, it is difficult to reproduce during verification tests.

The low maturity level of the blast wave modeling in the closed environment, the fact that the covers to be broken or ruptured by the blast effect are mostly produced from hyperelastic material, and the difficulties of the hyperelastic material behavior in mathematical modeling can be listed as disadvantages. Tactically, it is also one of the disadvantages that it can be observed by enemy forces that the ammunition is fired and the canister is now empty.

On the other hand, it is among the advantages of the covers that they do not require maintenance and that they are light compared to electromechanical and mechanically driven covers. In addition, they are preferred because of their low system complexity and high reliability coefficients. In the event of a possible failure, the canister cover can be broken or ruptured by the missile and the task can be performed. However, it cannot be guaranteed whether the mission will be successful or not due to the impact loading.

2.1.4. Covers Broken by Radome Impact

Missile seekers play a crucial role in guiding missiles to their targets and are often made of glass ceramics for several reasons. Firstly, glass ceramics have a high strength-to-weight ratio, which makes them ideal for use in missile seekers that must endure the intense G-forces of flight. Secondly, glass ceramics have excellent thermal stability and can maintain their properties over a wide range of temperatures, which is crucial for the operation of missile seekers in extreme environments. Additionally, glass ceramics are highly transparent and have low light absorption, making them suitable for use in optical systems such as those used in missile seekers. Lastly, glass ceramics have a high

resistance to chemical attack, ensuring the long-term stability and reliability of the seeker system. [5]

On the other hand, glass ceramics have several disadvantages when used as missile seekers. Firstly, they are more expensive compared to other materials, making them a less popular choice for some applications. Secondly, glass ceramics are fragile and can easily be damaged under high stress or impact. This makes them unsuitable for applications where the material will be subjected to high levels of stress or impact. Additionally, the manufacture and processing of glass ceramics is challenging and requires specialized equipment and techniques. This makes it difficult to produce these materials in large quantities. Finally, glass ceramics are not as widely available as other materials, which can make it challenging to source the material for use in missile seekers. Furthermore, they are relatively heavy compared to other materials, making them unsuitable for applications where weight is a critical factor. [6]

The table showing the material properties belongs to Pyroceram Code 9606 product (Corning Inc.) was as follows. Also, datasheet supplied by the company is given in Appendix 1. [5]

Table 1 Pyroceram Code 9606 Material Properties [5]

Physical Properties	Value	Properties
Water Absorption	< 0.01	%
Softening Point	1350	°C
Gas Permeability	Impermeable	
Density	2.6	g/cm^3
Elastic Modulus	120 x 10^6	kPa

Thermal Properties	Value	Properties
Coefficient of Linear Expansion	57X10^-7	1/ °C
Thermal Conductivity	0.0081	cal/(s x cm x °C)
Thermal Diffusivity	0.0127	cm^2/s
Specific Heat	0.233	cal/(g x K)

As a result of the contact of the radome with the cover, the ceramic part will be subjected to dynamic loading. How much this load is will play an important role in whether the missile can fulfill its task. The loading that will occur with the contact of the radome with the cover will be an input to the fracture analyzes to be carried out for the glass ceramic part. Also, it is important to consider this impact load in the design and engineering of solid military rockets to ensure their structural integrity and reliability during flight.
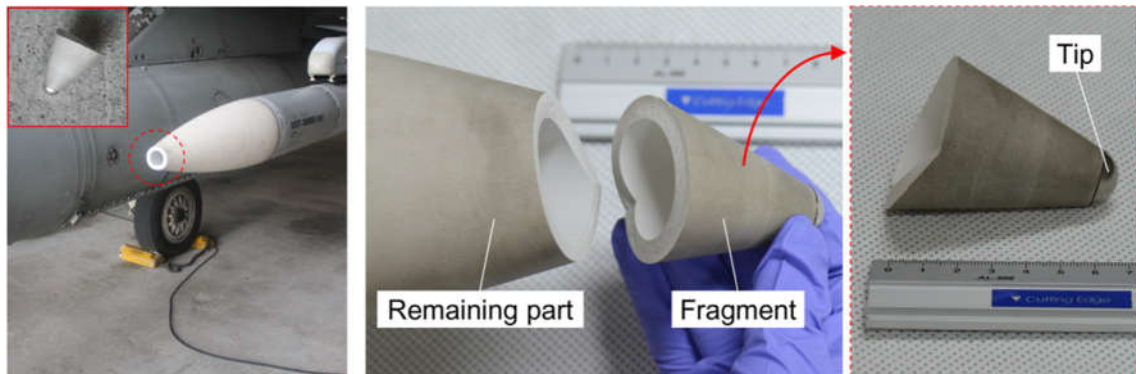
Figure 5 Loss of Structural Integrity of the Ceramic Glass Seeker [6]

The covers must be designed to break in a predefined direction and under a specified load. They are subjected to a pre-load in the form of a blast wave and are expected to break upon random impact, with the breaking point located in an area of stress concentration as per the design principle. Missile impact causes damage to canister covers, which are typically constructed from foam materials for their superior cushioning and impact absorption properties.

Figure 6 Broken Foam Canister Cover Parts Belongs to Sea Sparrow Weapon System [7]

Foam materials, due to their porous structure, tend to have high gas permeability. This means that gases can easily pass through the foam material, which can be problematic in applications where a gas-tight seal is required. To address this issue, additional layers are often added to the foam material to reduce gas permeability and achieve a desired level of sealing. These additional layers can be made of different materials, depending on the specific requirements of the application. They are unlikely to provide significant Electromagnetic Interference (EMI) and Electromagnetic Compatibility (EMC) protection on their own. Foam materials are not effective at blocking or absorbing electromagnetic fields, and therefore they can be used with other materials aluminum, copper typically.

2.1.5. Pyrotechnic Containing Canister Covers

The front cover, which is detonated by the current given just before the firing sequence, is separated from the canister structure. Although there is no possibility of nose contact with the missile, this explosion, which occurs right in front of the part containing the avionics of the missile, can create negative effects. It can be listed as the progression of solder cracks on electronic cards and the separation of large card pieces on the PCB from the card.

Pyrotechnic applications are frequently encountered in the aerospace and defense industries. Although there are not many error records in open sources about system failures, it causes catastrophic results in case of it. The most important example of this is PSLV-C39 pyro bolts not working on 31 August 2017 due to thermal load. The task performed resulted in the LV heatshield not working and the payload hitting the heat shield. 210 pyrotechnic elements were used in NASA's Apollo LV. [8]

In canister cover applications, the explosive placed in the cover in the form of a linear band is activated by electric current. A large number of tests are required to increase the reliability of the system against the case of not opening the cover. An example system resulting in the disassembly of the cover is given below.

2.2. Academic Studies

In the study conducted by Wonhong Choi, Sunghun Jung as the missile leaves, the interaction of the missile folding wings with the remaining parts on the cover frame was investigated. The research also shows that abnormal fastener installations and separations increase the support ring deformation induced by an interaction with the cover remains, triggering further interference with the boosters on the bottom of the missile. Additionally, the variation of material property in a high-speed environment is analyzed. In this context, simulation studies were carried out with Abaqus 6.14-1 finite element software, and its bad effect on the opening of the folding wing on the missile was revealed. [9]
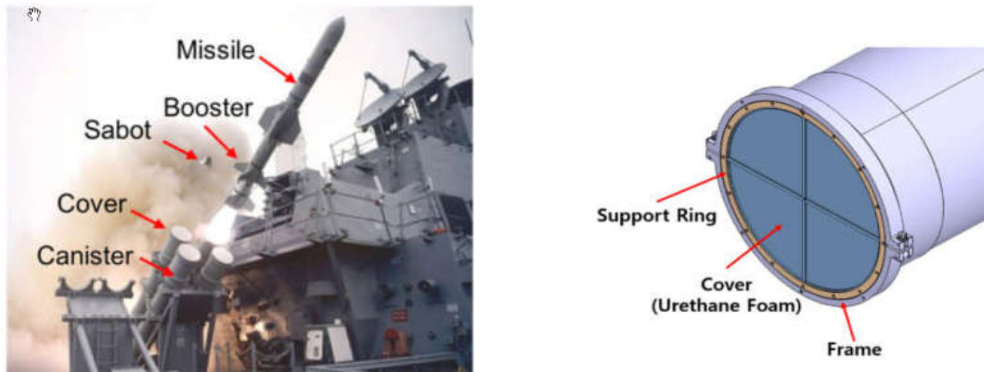
Figure 7 Firing of Harpoon Missile (Left) and Simplified CAD Isometric View (Right) [9]

The master study carried by Adeel K. M., analyzes a hollow beam and rigid body collision, which is then replaced by a foam sandwich beam with Polyurethane foam as a core material, considering both bonded and non-bonded foam with a coefficient of friction. The study evaluates two types of geometry for both hollow and foam sandwich beams, and two different densities of flexible polyurethane foam are analyzed to determine the dependence of results on foam density. The viscoelasticity of polyurethane foam is modeled using 8-term Prony series parameters, and the rigid polyurethane foam is modeled using P-alpha model and Hugoniot shock data [10]

In other sources, the covers used in canisters were collected in six classes. These are classified as mechanism activated caps, hard caps, diaphragm type caps, foam type caps, pyrotechnic caps and others. The study considered system level requirements during the design phase, and suitable composite materials and manufacturing methods were selected based on literature survey. Load levels were determined using experimental and analytical approaches, and finite element analysis was used to determine the design parameters of the cover. [11]
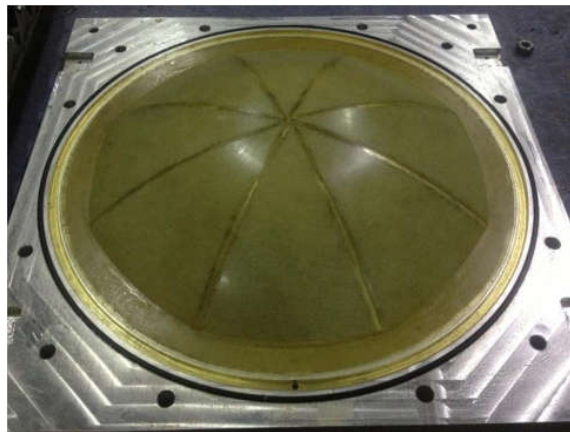
Figure 8 The Canister Cover Manufactured by Using Resin Transfer Method

Within the scope of the literature review, the design and production of the canister cover, which is designed with a numerical and experimental approach, in which light and directional fracture mechanics work, is included in the article published by Guangming Zhou, Deng'an Cai, Yuan Qian, Jian Deng, Xiaopei Wang. In the related study, cover composite hand lay-up technique and resin infusion process were used. During the composite design, the weakened region where the fracture will start was designed by using resin adhesive, and it was aimed to separate the polyurethane foam-on-epoxy-soaked glass fiber layer from the canister as a single whole. It is the sudden pressure pulse that occurs in the canister as a result of the missile firing that initiates the fracture mechanics. The impact of collision was not investigated in this study. [12]

Jae-Wook Chung, Sang-Mok Shim, Young-Gwan Bae conducted the research of the frangible canister front cover test bench. In this context, the distance between the actual

cover and the nose of the missile had to be increased in order for the test hydraulic test setup to be able to catch the missile canister cover collision speed. [13]
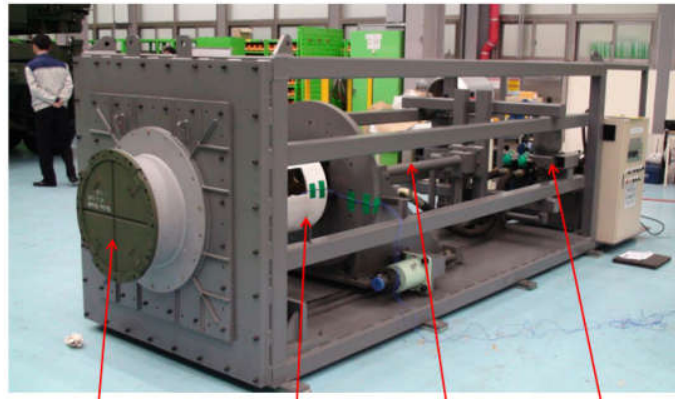
Figure 9 Fragile Canister Cover Test Bench [13]

Another study on the subject is T.Y.Kam, J.H. Wu, W.T.Wang is the determination of the external load required to break the frangible laminated composite cover in the previously determined direction. In this context, a theoretical and experimental approach has been made to break the canister cover, which consists of four layers and in the form of a convex, in a determined direction at a determined load. Since the cost of the test to be carried out with missile firing to reflect the real situation is very high, uniform pressure was applied and the results obtained were compared with the theory. [14]

The book "LASL Shock Hugoniot Data" by S. P. Marsh is a comprehensive collection of data on the behavior of materials under shock wave conditions. The data was compiled by researchers at the Los Alamos Scientific Laboratory (LASL) and covers a wide range of materials and shock wave conditions. This book serves as a valuable reference for researchers and engineers working in fields such as materials science, aerospace engineering, and defense technology. [15]

3. DETERMINATION OF THE LOADS

3.1 Loads Acting on the Canister Covers After Rocket Ignition

The canister is exposed to various loads and environmental effects throughout its life cycle. These are thermal, dynamic, static loads. However, unlike the loads that the missile is exposed to during its life cycle, the loads required within the scope of this study are the loads that affect the canister cover after engine ignition. Loads affecting the canister cover after engine ignition can be grouped into 3 categories.

- Air-Blast Effect
- Radome Impact
- Exhaust Gas Effect on Adjacent Launch Canister Cover

While making this listing, it has been assumed that the dynamic effect of the exhaust gases coming out of the missile nozzle inside the canister has not yet reached the front cover. For this, the distance between the missile radome and the front cover must be short.

Internal and external loadings are so fast that the effect of inertia forces and stress waves on the material cannot be ignored. In short, the loads acting on the cover can be classified as dynamic loading. In this section, prestressed explicit analysis is will be run with the forces obtained. The loads to be used within the scope of the analyzes to be carried out must be calculated, created by the analysis method or obtained by the test method.

3.1.1. Air-Blast Dynamic Pressure Measurement

The pressure is at ambient until the air-blast arrives. At this time, it instantaneously rises to its peak side-on overpressure, decays back to ambient, drops to a partial vacuum, and eventually returns to ambient. [16]
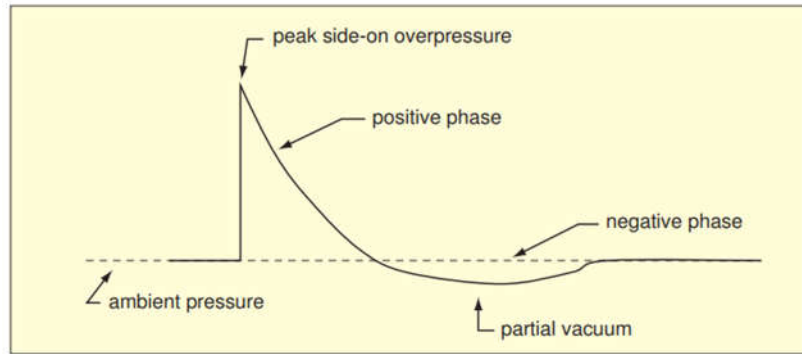
Figure 10 Overview of the Air Blast Wave [16]

It is crucial to accurately measure the dynamic pressure produced by air-blast and evaluate its impact on structures. The pressure data of the blast wave stem from the engine ignition are collected with dynamic pressure gauges. The blast wave is damped by interacting with the canister internal structure. However, due to the speed of the blast wave, it is important how often the data will be collected. Dynamic pressure gauges with High Response frequency should be used. It is also necessary to filter the data collected with high frequency.

In addition to all these, the position of the dynamic pressure gauge should be as close as possible to the canister cover. The placement of the dynamic pressure sensors is shown in the Figure 10. The measurement was carried out using more than one sensor, considering the possibility that the test is not reproducible and that the particles in the exhaust gases may adhere to the sensor diaphragm and cause the sensor to become saturated.
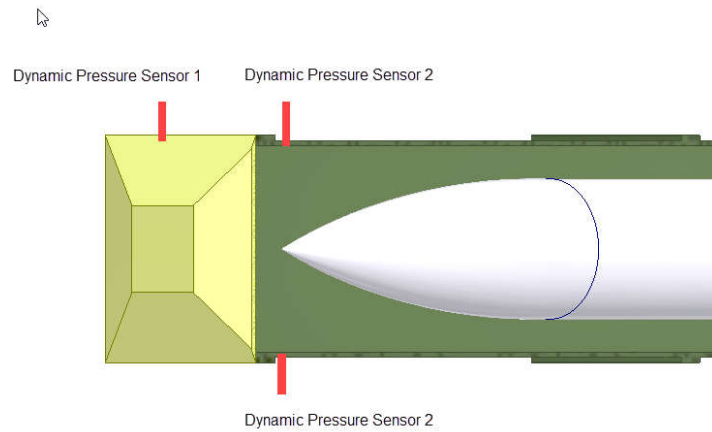
Figure 11 Dynamic Pressure Placement in Missile Firing Test

The sensors used for the measurement of pressure waves at high frequencies generally have piezoelectric and mems technologies. The properties belong to the sensor used are given in Table 2. In addition, the data sheet of the sensor is given in Appendix 2. The sampling rate has been determined as 100 kHz. High pass filter is preferred in order to avoid noise in high frequency measurements.
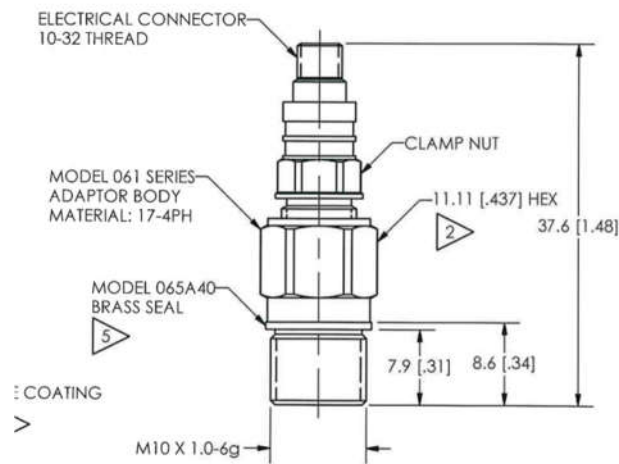
Figure 12 Schematic View of Dynamic Pressure Sensor [17]

Table 2 General Properties of the Dynamic Pressure Sensor [17]

Performance

Sensitivity	3.6 mV/kPa
Maximum Pressure	6895 kPa
Resolution	0.007 kPa
Resonant Frequency	≥500 kHz

Physical

Sensing element	Quartz
Diaphram	Invar

Rocket development testing is a crucial aspect of ensuring the reliability and safety of a rocket prior to launch. During these tests, air blast measurement is performed to evaluate the dynamic pressure generated by the rocket engine exhaust gases. The results of these tests are displayed in a graph, which shows the time taken for the pressure wave to reach the front cover of the canister, after the air blast wave has passed. The pressure wave, followed by a vacuum effect, behaves similarly across all three sensors, as can be seen in the graph. After the pressure wave caused by the movement of the missile and the exhaust gases, the pressure level is equalized with the ambient pressure.

Before the effect of the exhaust gases, a collision occurs between the missile radome and the cover, and therefore, this effect is not considered in the study. Also, the measurement taken for air blast will be utilized in future works. It is not feasible to pressurize the canister cover to the air blast pressure level in the current testing setup. Therefore, a simulation study that can be validated with testing will be conducted. As a result, impact analysis is performed using an explicit integration method, which will be further discussed in subsequent sections of the thesis.
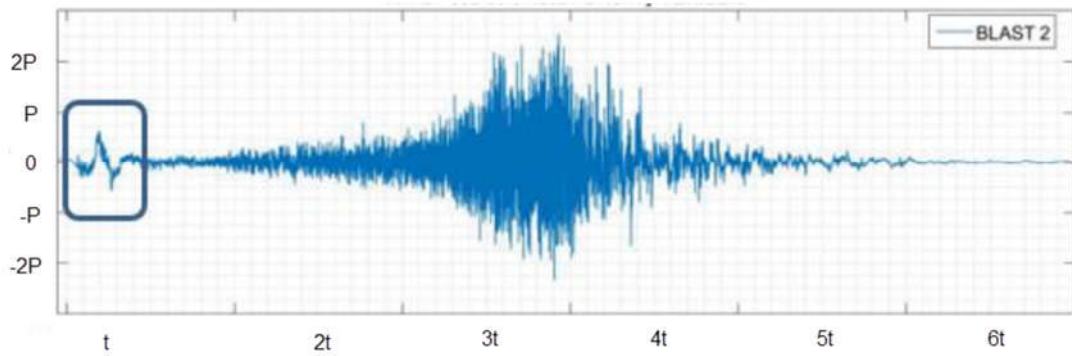
Figure 13 Collected Data During Firing Test

3.1.2. Radome Impact Velocity

The grain refers to the shaped mass of processed solid fuel inside the rocket engine. The performance characteristics of the engine are determined by the fuel material and the geometric design of the grain. The burning area may or may not change over time, depending on the specific molding and design of the solid fuel rocket engine. The thrust force can be classified as aggressive, neutral, or progressive, and its variation is illustrated in a graph. [18]
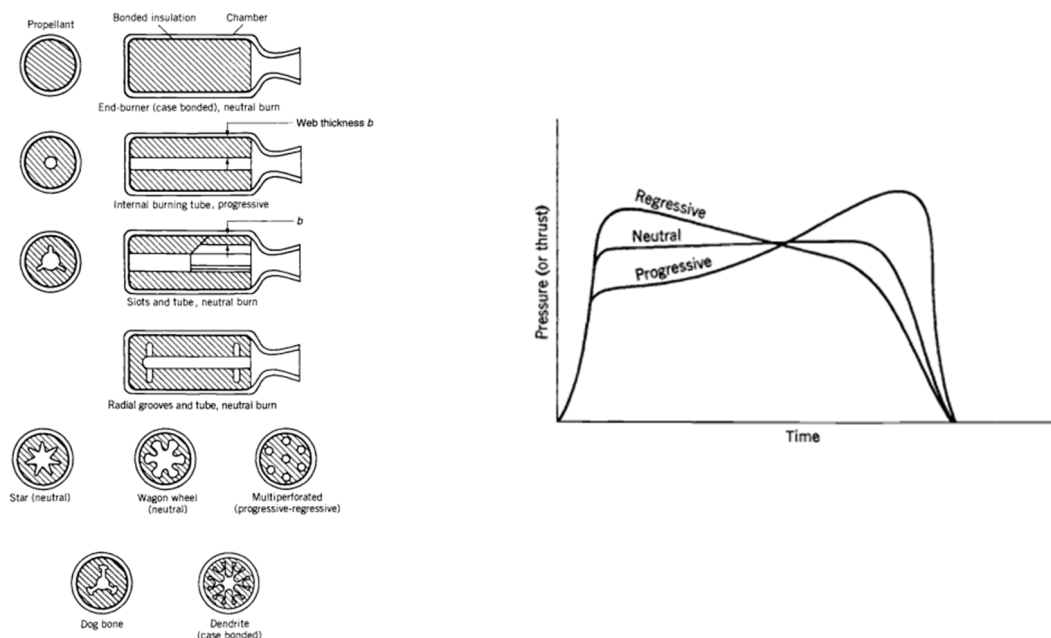
Figure 14 Geometric Design of the Grain (Left), Trust Force vs Time Graph for 3 Different Grain (Right) [18]

The relation between the performance of a propellant and the principle of conservation of matter states that the mass of propellant burned in a unit of time must equal the sum of the change in gas mass per unit of time within the combustion chamber grain cavity and the mass flowing out of the exhaust nozzle per unit of time. [18]

$$\dot{m} = A_b r \rho_b \tag{1.a}$$

$$A_b r \rho_b = \frac{d}{dt}(\rho_1 V_1) + A_1 p_1 \sqrt{\frac{k}{RT_1}\left(\frac{2}{k+1}\right)^{(k+1)/(k-1)}} \tag{1.b}$$

The fixed shape of the nozzle and fluctuations in atmospheric pressure caused by changes in altitude can create a discrepancy between the external atmospheric pressure (p_3) and the internal pressure (p_2) of the hot gas jet at the nozzle exit. As a result, in a rocket propulsion system that operates steadily while moving through a uniform atmosphere, the total thrust is equal to the equation below.

$$F = \dot{m}v_2 + (p_2 - p_3)A_2 \tag{2}$$
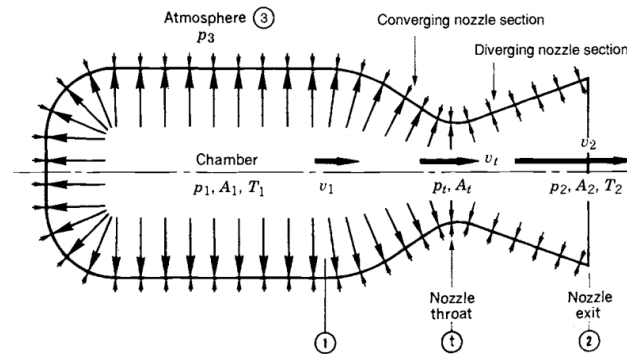
Figure 15 Overview of the Solid Propellant Rocket Engine

It is known that many companies operating in the military field perform internal ballistic analyzes with the vehicles they have developed. But it is available in open source programs for use in development work. The most important of these are the programs developed for chemical balance before and after combustion.

In chemical equilibrium, a reaction system reaches a state in which the rates of the forward and reverse reactions are equal, and the concentrations of the reactants and products remain constant over time. CEA uses this concept to predict the composition of a mixture of gases or liquids at a given temperature and pressure, considering the chemical reactions that occur.

In design and analysis applications to mechanical systems involving reactive mixtures, it is highly beneficial to be able to determine the chemical equilibrium compositions of the reactive media. Mechanical systems include aircraft combustors, rocket motors, gas turbines, shock tubes, and so on. For more than decades NASA Lewis Research Center have made great efforts in developing methods and computer programs for calculating complex chemical equilibrium compositions, as well as thermodynamic and transport properties of mixtures. Many versions of their programs have been adopted for research studies, development work and the latest version is called CEA (Chemical Equilibrium and Applications). [19]

As may it seen, thrust force is a function of time. In stop and start of the motor ignition, can be named as a transient region, trust force is not constant instead graph is so steep. This is usually due to the burning rate of the solid fuel grain changing or the geometry of the grain being altered, causing a fluctuation in the pressure and velocity of the hot gases being expelled from the engine.
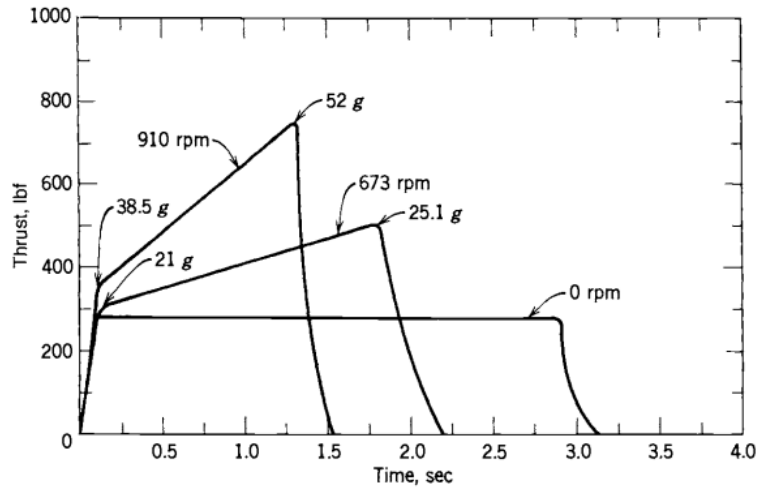
Figure 16 Transient and Steady State Trust Force [18]

However, a significant part of the missile's movement in the canister passes through the transient region. The formulas mentioned above are valid for steady state. Transient region modeling is more complex. Therefore, static ignition tests are inevitable.
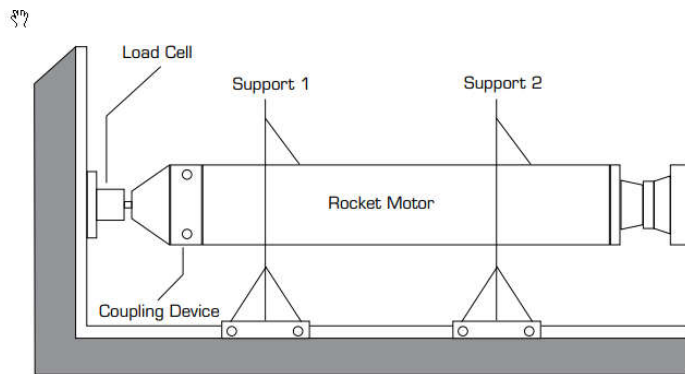
Figure 17 Static Firing Test Set Up [20]

The trust force for the transient region is obtained by amplifying and filtering the data obtained from the load cell. Thus, with the changing mass, the acceleration profile of the missile in the canister is obtained.
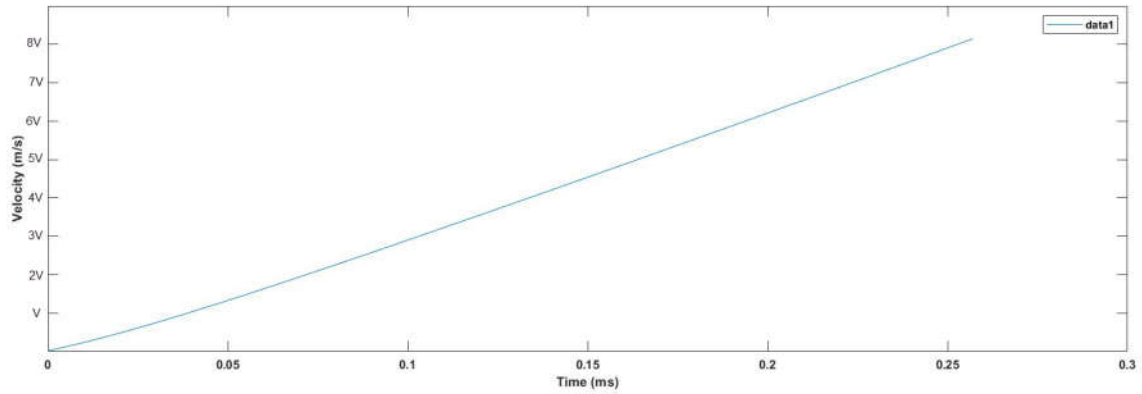
Figure 18 Velocity of the Missile in Canister

Due to the increasing momentum of missile, the distance between the radome and the canister cover is kept as short as possible. Otherwise, the missile's momentum increases before collision, which increases the chance of the radome taking damage from the collision.

3.1.3. Exhaust Gas Effect on Adjacent Launch Canister Cover

More than one canister is loaded on a launch vehicle due to tactical requirements. This gives the user an operational advantage. Immediately after the missile leaves the canister, rocket engine exhaust gases have effects on the adjacent canister cover such as pressure, temperature, acidity and toxicity.
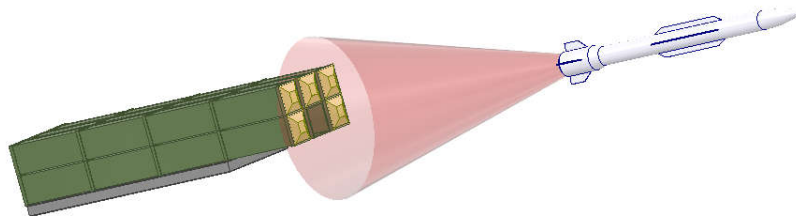
Figure 19 Exhaust Gas Affecting on Adjacent Canister Firing

The canister cover is expected to withstand a specified number of firing loads over its life cycle. The system integrity of the cover exposed to external loading must be maintained. It is expected that the canister front cover will withstand the loads created by firing the missile in the adjacent canister while aiming to break it with the contact of the radome with the cover at the determined low loads.

There are various studies in the literature to obtain the pressure control from the effect on the adjacent canister. If one missile leaves the canister, the pressure acting on the side canister cover increases to a certain extent as the missile moves away from the canister and then decreases. [21]

L_{ex} (m)	P_{max} (MPa)	T_{max} (K)
5	0. 1013	310
10	0. 1019	448
20	0. 1039	538
25	0. 1028	472

a 5m   b 20m   c 25m
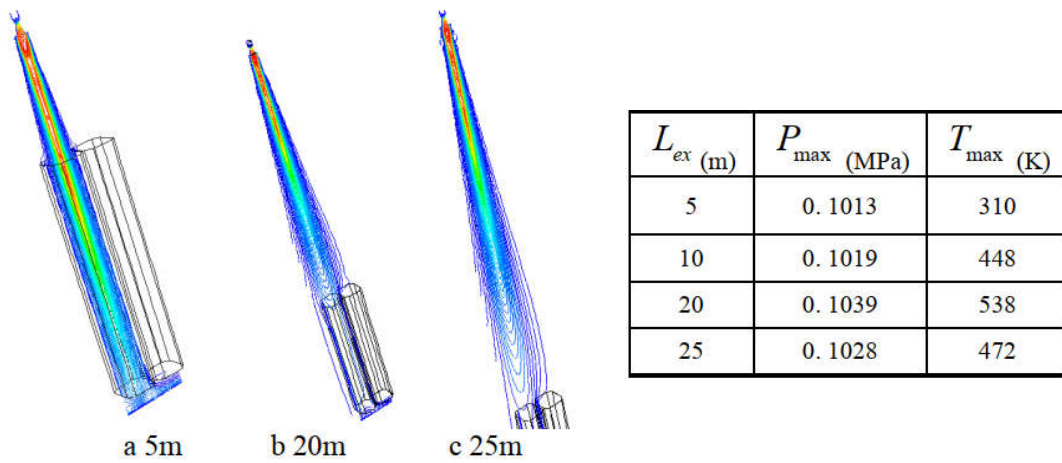
Figure 20 CFD Analysis on 5m (a), 20m (b), 25m(m) and Pressure Acting on Adjacent Canister Cover (Right) [21]

To understand and evaluate the fluid dynamics and heat transfer of rocket engine exhaust gases, specialized software tools are employed. Despite the high temperature of the exhaust gases, the temperature rise in the canister cover is minimal due to the short duration of exposure. Following the engine ignition, the missile accelerates rapidly. As a result, the heating effect was not considered during the structural analysis of the front cover of the canister.

The findings from the analysis need to be validated using data collected from firing tests. There are various methods in the literature to measure engine exhaust gas pressure. The scope of the study, unlike rocket engine development activities, is the effect of rocket

engine exhaust gas on the canister front cover. For this reason, it was built on the measurement of structural displacement and it was decided to collect strain gauge data.

However;

- The changes in temperature can affect the resistance of the strain gauge, leading to inaccuracies in the measurement data.
- The surface should be roughened to provide a better surface for the strain gauge to adhere to. However, due to the nature of the foam material, there is surface roughness.

A methodology has been established to perform the measurement using a strain gauge.

- Instead of a foam material with a convex shape, a flat metal plate was selected as the measuring surface to ensure linear behavior.
- The CFD analysis revealed that the pressure decreases with increasing radial distance from the nozzle axis. As a result, the strain gauges were positioned near the nozzle axis to accurately capture the strain.
- To account for the fact that the test could not be repeated, multiple strain gauge placements were utilized.
- To measure strain in multiple directions, strain gauge rosettes were employed.
- In order not to be affected by the temperature rise and not to be affected by the unburned aluminum particles in the exhaust gas during the measurement, strain gauges are attached to the inner surface of the canister instead of the outer surface.
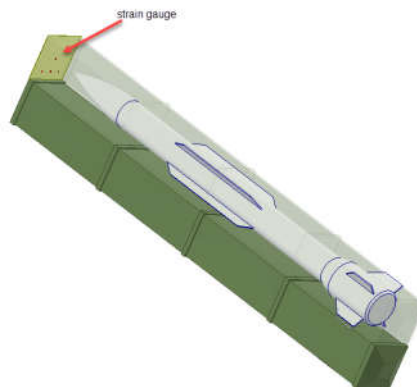
Figure 21 Placement of the Strain Gauges during Firing Test Activity

The Ansys Linear Static Analysis tool was employed to automate and repeat simulations by changing the pressure design parameter. The strain value of the plate was identified as the output parameter and the simulation was terminated when this value matched the measured value. The results obtained correlate with the results performed by MA Yanli, JIANG Yi, HAO Jiguang, and YAN Feng. It was not included in the structural analysis studies because the loading is between 1 and 2 kPa and it imposes a loading that closes the notches on the cover. [21].

4. MATERIAL CHARACTERISATION AND PRODUCTION

Incorrect material selection can have disastrous consequences such as the front cover of the canister becoming stuck to the missile body, obstructing the unfolding of the wing or causing harm to the seeker. The frangible cover should break apart into only a limited number of large fragments and none of these fragments should stay in the flight trajectory. As previously stated in the thesis, the glass ceramic composition of the seeker demands that any collisions be effectively absorbed and cushioned to safeguard against damage.

This section focuses on the studies performed regarding the characterization of the foam material obtained.

- Rigid Polyurethane Production
- Material Characterization Tests

4.1. Rigid Polyurethane and Production

Rigid polyurethane is commonly used in the industrial applications. Especially in construction, automotive and clothing industry. Mixture of isocyanate, polyol, blowing agents and catalyst is to be pressurized before the pouring into die. Curing time approx. less than 1 hour. The machine used for mixing operation is given in the Figure 21. [22, 23]

Figure 22 Low- and High-Pressure Dosing Machine Developed by Canon Afros Company [23]

Mechanical properties of foam directly linked to cellular structure of foam. Closed cell foam is more rigid compared to the open cell foams. Open cell foams are more flexible. In order to clearly understand microstructure of the foam, cellular morphology should to examined with scanning electron microscopy.
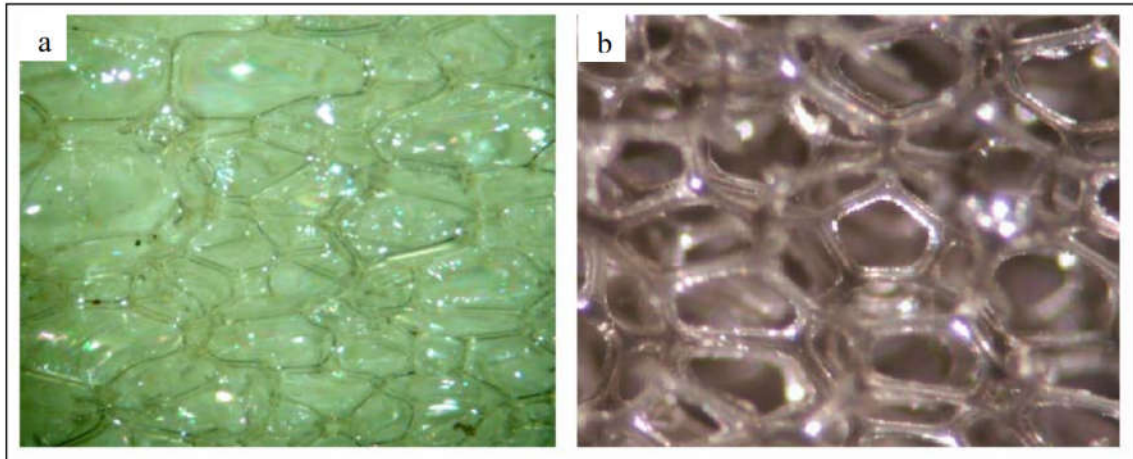
Figure 23 Closed (Left) and Open (Right) Cellular Structure of the Polyurethane [24]

Although the scope of this thesis is limited to rigid polyurethane material, some of the cells in the material after the pouring process are expected to be open cells.

The design and production of the aluminum mold of the polyurethane casting mold was carried out. Since the notch depths on the product will be verified by testing and analysis, a modular mold design has been made. The parts determining the depth of the notches on the product are replaceable.
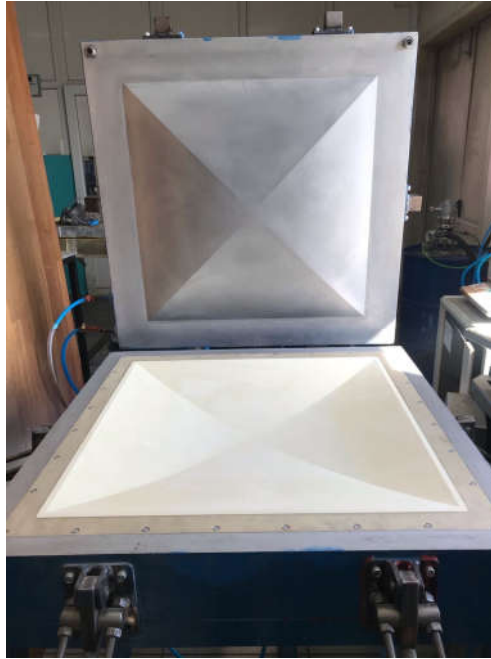
Figure 24 Manufacturing of Polyurethane Layer with Mold

In order to establish the production process, trial productions were accomplished. At the end of these trial productions, it was clarified how much the mold should be heated before casting, the methodology required to separate the product from the mold surface, and the pressure at which the mixture should be prepared before casting and curing time. For this reason, many trials have been produced. As stated in the later parts of the thesis, a mixture of isocyanate, polyol, blowing agent was poured into the mold to provide a density of 160 kg/m^3.
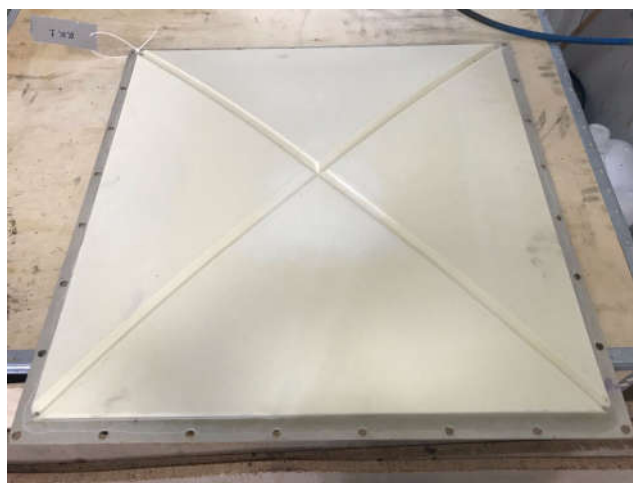
Figure 25 Extracted Product from Casting Mold

Additionally; The sabot design has been carried out in order to bedding the collision, to ensure that the radome of the missile can contact the cover missile at a certain point, to reduce the speed in the collision of the missile with the cover, and to distribute the load on the cover almost equally. According to the data obtained in the test studies, a separate mold was designed and produced for the sabot due to the possibility of making structural changes and the ease of prototype production. After the validation of the product, a single mold will be designed and produced without mass production.

Figure 26 Aluminum Casting Mold for Manufacturing of Sabot

4.2. Material Characterization

Characterization tests were carried out to determine the properties of the material. Information on which tests were carried out is given in Table 3. Although the rigid polyurethane material showed viscoelastic behavior, the dynamic mechanical analysis test could not be performed.

Table 3 List of Performed Test to Determine Material Properties and the Standards

No	Test	Standard
1	Uniaxial Tensile Test	STANAG 4506 ED1
2	Moisture Absorption Properties	ASTM D 5229 M (2004)
3	Density	ASTM D 792
4	Specific Heat Thermal Expansion Thermal Conductivity Glass Transition Temperature Degredation Temperature	ASTM D 3418
5	Compression Test**	-
6	Shore (A) And Shore (D) Hardness	ASTM D 2240
7	T-Peel Test	ASTM D 1623 TYPE C
8	Fracture Toughness	ASTM D 5045 /ASTM E 399

** R.D. Widdle Jr., et al, 2007, "Method II, relative positions of material points [25]"

Although the tests listed below have been performed, it is known that the thermal effect is low due to adjacent canister firing. For this reason, in this part of the thesis, the data to be used in the analysis study is emphasized. These;

- Uniaxial Tensile Test
- Uniaxial Compression Test
- Density
- Durometer Hardness
- Fracture Toughness

Since this data concerning the material cannot be acquired through open-source research, it was necessary to conduct a material characterization study. The outcomes of these tests will be employed to establish the essential material library for finite element analysis.

4.2.1. Uniaxial Tensile Test

Five dog bone-shaped specimens were fabricated from rigid polyurethane to evaluate their tensile strength and deformation characteristics. The specimens were stamped using a specific die, as illustrated in Figure 26. The uniaxial tensile test was carried out at a

constant speed until the specimen fracture. The strain and stress values were recorded and the test data is presented in the Table 4.

Figure 27 Uniaxial Tensile Test and Die Used for Extracting a Sample from Bulk

4.2.2. Uniaxial Compression Test

This test was performed to provide information regarding mechanical behavior of the rigid polyurethane. Compressive stress and strain data were recorded during the test. The produced test specimens were shown in the Figure 27. According the test data, the material shows orthotropic behavior contrary to expectation. After a short review, it is recognized that the specimen was extracted from the closed to molding wall. It was understood that the tested samples had a surface contacting to the casting mold and the wall formed on this surface showed. For that reason, the samples exhibit orthotropic behavior. Therefore, the tests were repeated. The new samples were extracted from the casting mold with no walls on the outer surface. The extracted samples show similar mechanical behavior in all three directions.
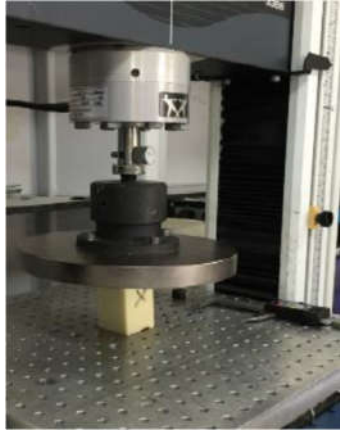
Figure 28 Uniaxial Compression Test

The determination of Poisson's ratio through compression testing is a widely utilized approach. However, the deformation of the material and the change in shape under load, such as barrel distortion, often necessitates alternative methods to be pursued. At this stage, a literature review was carried out.
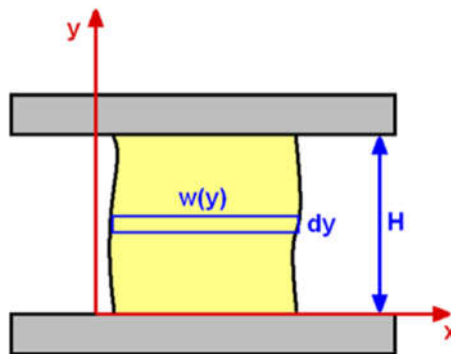
Figure 29 Shape Change of the Loaded Sample During Compression Test [25]

In the study conducted by R.D. Widdle Jr., et al, 2007, "Method II, relative positions of material points" was determined as an alternative method to the test ASTM 1621 D. Although this method was developed for flexible foam material, the potential of this method as an alternative has been evaluated for rigid polyurethane. With this method, the calculation of the Poisson ratio is performed by the displacement of the defined points on the test specimen. During testing, samples were compressed up to 5%, 33%, and 66% levels. Each compression level was held for 30 min for stress relaxation. [25]
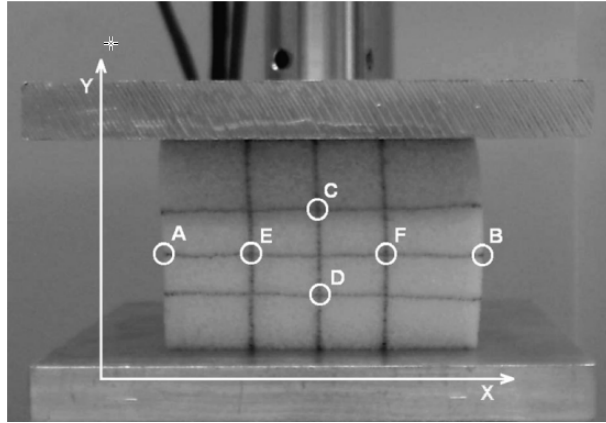
Figure 30 Alternative Methodology Offerred by R.D. Widdle Jr., et al, 2007, "Method II, Relative Positions of Material Points [25]

Strain rate calculated over the points remaining inside, instead of the points close to the corners on the surface of the test specimen. [25]

$$\varepsilon_y = \frac{|C - D| - |C_0 - D_0|}{|C_0 - D_0|} \tag{3.a}$$

$$\varepsilon_x = \frac{|E - F| - |E_0 - F_0|}{|E_0 - F_0|} \tag{3.b}$$

Poisson's ratio is a mechanical property of materials that describes the relationship between the lateral (transverse) strain and the axial (longitudinal) strain in a material when it is subjected to tension or compression.

$$v = -\frac{\varepsilon_x}{\varepsilon_y} \tag{3.c}$$

Unlike Method II, MATLAB image processing tool was not used. Same procedure defined in Method II was performed with the Instron test fixture with advanced video extensometer. Although it has the ability to take images at high speed, certain percentages of compression were applied for stress relaxation, and the test specimen was loaded with a low compression rate.
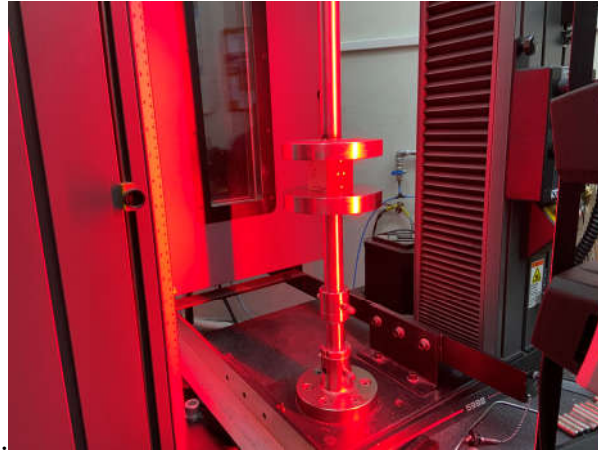
Figure 31 Application of Method II with Instron Test Fixture - Video Extensometer [26]

4.2.3. Density

Density of test specimen were determined according to ASTM D792 "Standard Test Methods for Density and Specific Gravity (Relative Density) of Plastics by Displacement". The density of water at 23 ˚C is 997 kg/m^3. The test methodology based on the volume of transferred water due to immerged test specimen. A pycnometer with temperature control is used as a test fixture.

4.2.4. Durometer Hardness

The standard ASTM D 2240-15 "Standard Test Method for Rubber Property – Durometer Hardness" covers twelve different type of hardness measurement device; Types A, B, C, D, DO, E, M, O, OO, OOO, OOO-S, and R. The measuring foot is pressed against the surface of the material with a specific force. The hardness of the material is then determined by the indentation depth or the resistance of the material to the indentation.
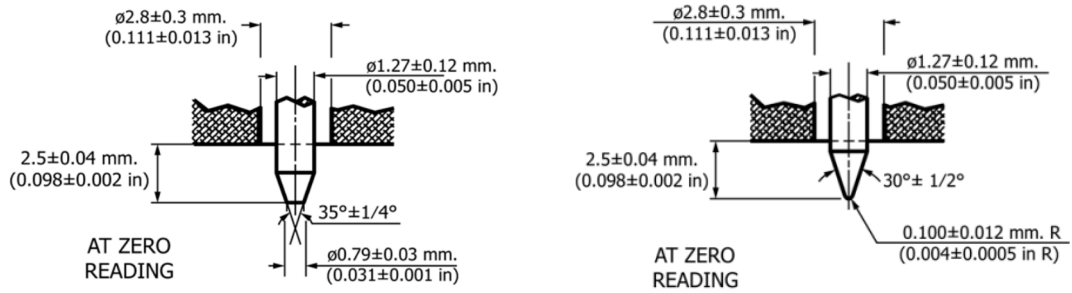
Figure 32 Measuring Foot for Durometer Hardness A (Left), Durometer Hardness B (Right) According to ASTM D 2240-15

4.2.5. Fracture Toughness

The specimens to determine fracture toughness according to ASTM D5045 "Plane-Strain Fracture Toughness and Strain Energy Release Rate of Plastic Materials were produced with following methodology. After molding a polyurethane, the specimen brings to desired geometry with CNC machine operation. The validity of the test directly depends on the sharp crack condition created in manufacturing. The specimens for single edge notch bending test are shown in Figure 32.
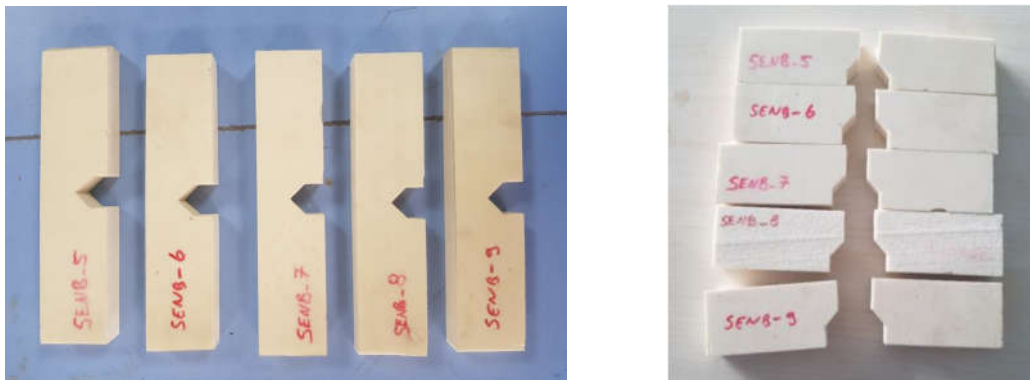
Figure 33 Fracture Toughness Test Samples (Left), Fractured Samples After Test (Right)

Also, it is important to note that the fracture toughness of foam materials can be highly dependent on the loading conditions and the presence of microstructural features such as pores, voids, and inclusions.

The stress concentration that will occur at the crack tip depends on the force to be applied and the crack geometry. In linear elastic fracture mechanics, cracks can propagate in three different ways: Mode 1: Opening Mode, Mode-2: Sliding Mode and Mode-3: Tearing Mode. Crack propagation can occur with one of the above-mentioned mode or with a combination of different modes.
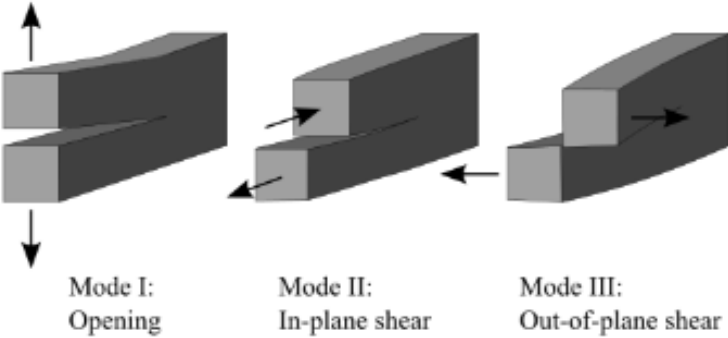
Figure 34 Fracture Modes [27]

4.2.6. Test Results

The prepared samples were tested in accordance with international standards. The data obtained as a result of the test are gathered together in the Table 4.

Table 4 Material Properties Test Results

No	Test	Standard	Results	
1	Uniaxial Tensile Test	STANAG 4506 ED1	Young Modulus	66 Mpa
			Strain	8%
2	Density	ASTM D 792	160.32 kg/m^3	
3	Compression Test	ASTM D 1621	Compressive Strength	3.3 MPa
			Strain	40%
4	Poisson Ratio w Compression Test*	-	Ratio	0.317
5	Hardness	ASTM D 2240	Shore (A)	95
			Shore (D)	41
6	Fracture Toughness	ASTM D 5045 /ASTM E 399	Stress Integrity Factor	59 MPa.mm^0.5

*Adaptation of method developed in the study conducted by R.D. Widdle Jr., et al, 2007 [25]

5. FINITE ELEMENT ANALYSIS

Throughout the preceding chapters of the thesis, various applications of canister cover were highlighted and the methodology for gathering material and load data for the analysis study was outlined. The focus was also on identifying the loads that impact the front cover of the canister and determining the standards for evaluating the mechanical properties of the newly developed material. The study utilized the Ansys FEM software to investigate the solid mechanics behavior and perform numerical simulations of the impact scenarios.

5.1. Explicit Integration Methods

Numerical solution of dynamics systems can be solved either in frequency or time domain. Solution stability, computational performance and accuracy are important parameters while selecting solution the domain.

Structural behavior of the canister cover with contact of the seekers radome can be modeled as 2nd Order Differential Equation in time domain. M, C and K matrices stands for inertia, damping and stiffness of the system. These three matrices may or may not be constant. It directly depends on the application. In case of large deformation K matrice also depends on the displacement. U notation commonly is used to represent deformation in the system. The notations $\dot{u}$ and $\ddot{u}$ are deformation velocity and acceleration, respectively. F represents the time dependent force vector acting on the system.[28]

$$[M]\{\ddot{u}\} + [C]\{\dot{u}\} + [K]\{u\} = \{f(t)\} \tag{4}$$

There are too many numerical solutions are available like The Newmark, Hilbert-Hughes-Taylor, Newton etc. However, time integration methods can be divided in two categories which are implicit and explicit. Even if the numerical methods used one or more previous solutions, the key difference between these methods lay on whether using next step solution's derivatives or not, while finding the next step.
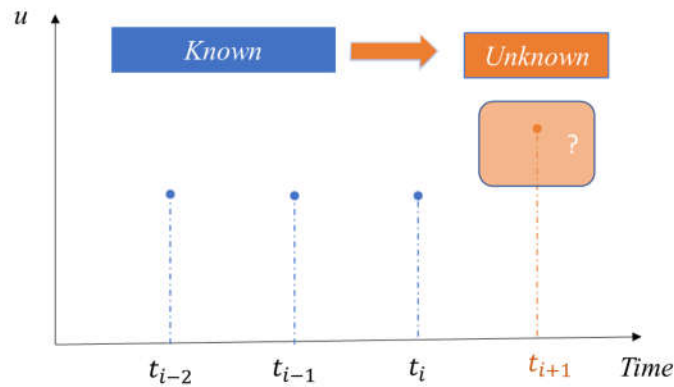
Figure 35 Implicit or Explicit Time Integration [29]

Whereas in implicit time integration method, next/unknown step solution is found by using derivative at next/unknown time step, the explicit time integration method uses the known/current time step solution. In other words, whereas the implicit integration methods require one or more iterations in one-time step, the explicit method does not require an iteration. For that reason, the explicit integration method is computationally effective. If the implicit methods are preferred to use instead of explicit method, solution time gets longer and longer. And as a matter of fact, that, computation might be fail in most engineering application.

Explicit integration method can be calculated within the shorter time. In other words, the engineering problems in which the force acting on the system in short period of the time like impact, penetration, crash, shock wave propagation, buckling, instantaneous failure of the material etc. However, in order to guarantee the convergence, you need to use small step size.

The duration between the successive iteration is called integration time step. In order to guarantee the convergence of the solution in explicit method, time step is limited by the Courant-Friedrich-Levy condition. It is abbreviated as a CFL Condition. Courant-Levy, et al stated in their work the time step must be limited so that a stress wave cannot travel further than the smallest element characteristic length in mesh. [30]

$$\Delta t \leq f * \left[\frac{h}{c}\right]_{min} \tag{5.a}$$

In formulation, h, c and f corresponds to characteristics length of the element, material sound of speed and safety factor. F is safety factor is equal to 1, usually lower than 1. While the sound of speed is material property, characteristic length of the element is directly relevant the mesh used on the model. Material sound of the speed may not be available in open source. If it is not possible to find with test, the formulation can be used for approximation.

$$c = \sqrt{\frac{E}{\rho}} \tag{5.b}$$

E: Young Modulus

C: Wave speed

$\rho = Density$

Characteristic length of the mesh element has a direct affect to times steps require to solve model. That is the main reason why the element needs to be equal in size as much as possible. Otherwise, the smaller element taking place in mesh of the model may results in a longer solution time. Calculation of the characteristic length of the mesh elements tabulated in Table 5.

Table 5 Characteristic Length of the Mesh Elements

Element Shape / Geometry	Characteristic Length
Hexahedral/Pentahedral	The volume of the element divided by the square of the longest diagonal and scale by $\sqrt{2}/3$
Tetrahedral	The minimum distance of the any element node to it's opposing element face
Quad Shell	The square root of the shell area
Tri Shell	The minimum distance of the any element node to it's opposing element edge
Beam	The length of the element

It is not easy to compare two-time integration method, by not taking account the engineering application area, nevertheless some parameters were listed in the Table 6.

Table 6 Basic Comparison of the Explicit and Implicit Integration Methods

	Explicit	**Implicit**
Stability	Depends on time step size	Unconditionally Stable
Time-Step Size	Very Small	Large
For Non-Linear Problem	Does not need iteration	Needs iterations
Solving Speed for One Step	Fast	Slow
Time Step Determination	Calcuated by Solver with CFL Criteria	Input by User/Default option of the solver

5.2. Explicit Dynamic Methods

The reason why the explicit dynamics solution is chosen can be listed as a large deformation and strain of canister cover with contact of missile radome, nonlinear material behavior of the foam material, failure, fragmentation and complex contact between radome and canister cover. The all load transfer and interaction is over in as short time.

5.3. Material Modeling

Material modeling will be examined in two parts as P-Alpha Model and Shock Equation State of Linear.

5.3.1. P-Alpha Model

The P-α compaction model, also known as the P-α model, is a theoretical model of ductile porous compaction materials that was developed by Hermann in the 1968 and Carrol and Holt (1972). The P-α equation of state, introduced by Herrman, was designed to characterize porous materials. It assumes that when a stress is applied, the material will initially respond elastically, but as the stress increases, the pores in the material will eventually be crushed, resulting in plastic compression that cannot be reversed. When the partially crushed porous material is unloaded, it follows a new elastic curve that is based

on the maximum stress it experienced. When the stress is high enough, all of the pores will be removed, and the material will behave like its original solid form, according to the P-α equation of state. [31, 32]

α is scalar variable and represents the ratio of the density of solid material to density of porous material. In this context, the subscript "s" indicates properties of the solid material, while the variables without a subscript relate to the properties of the porous media.

$$\alpha = \frac{\rho_s}{\rho} = \frac{V}{V_s} = \frac{V}{V - V_p} \geq 1 \tag{6}$$

When a material is fully compacted, the value of α is set at 1. On the other hand, if the material is not fully compacted, α will have a value greater than 1. This assumption is made under the premise that the density of the pores is so small compared to the solid phase that it can be considered insignificant.

An equation of for the pressure of the porous material as a function of

$$p = p(\alpha, \rho, E_m) \tag{7.1}$$

Assuming that the pores carry no pressure and applied pressure creates a corresponding pressure within solid phase equals to

$$p_s = \alpha p \tag{7.2}$$

The elastic curve originally was suggested by Hermann in 1968 is represented by a differential equation as [31]

$$\frac{d\overline{A_{El}}}{dp}(\alpha) = \frac{\alpha^2}{K_0}\left(1 - \frac{1}{h^2(\alpha)}\right) \tag{8.1}$$

$$h(\alpha) = 1 + \frac{(c_e - c_s)(\alpha - 1)}{c_s(\alpha_0 - 1)} \tag{8.2}$$

$$K_0 = \rho_{s0} c_s^2 \qquad (8.3)$$

c_e and c_s refers to reference sound of porous and solid material respectively. K_0 is bulk modulus of the solid material. For ease of computation elastic region is simplified and linearize by Wardlaw, et al. [33]

$$P_{el}(\alpha, \alpha_{min}) = \alpha_{min}\left(p - P_{pl}(\alpha_{min})\right)\frac{d\overline{A_{el}}}{dp}\bigg|_{\alpha=\alpha_{min}} \qquad (9.1)$$

The equation for the plastic curve

$$A_{pl}(p) = 1 + (\alpha_e - 1)\left(\frac{p_s - p}{p_s - p_e}\right)^n \qquad (9.2)$$

The described formulation of the elastic and plastic curves is given in the Figure 35. If it is needed to interpret the compaction behavior of the ductile porous material.

- α_0 corresponds to unloaded state
- α_e elastic limit where plastic deformation begins
- α_{min} after passing plastic region in case of unloading the state follow up new elastic curve called $A_{el}(p, \alpha_{min})$. In elastic region material shows some recovery. It ended up with different compaction value than α_{min}. α_{min} can be described as minimum value of α achieved by the material.
- As the α value approaches one, the slope of the elastic curve decreases. In other words, the slope of $A_{el}(p, \alpha_{min}^1)$ is less than $A_{el}(p, \alpha_e)$; in the same way slope of the $A_{el}(p, \alpha_{min}^2)$ is less than $A_{el}(p, \alpha_{min}^1)$
- When material is fully compacted, α reaches to 1 and p value leads to p_s
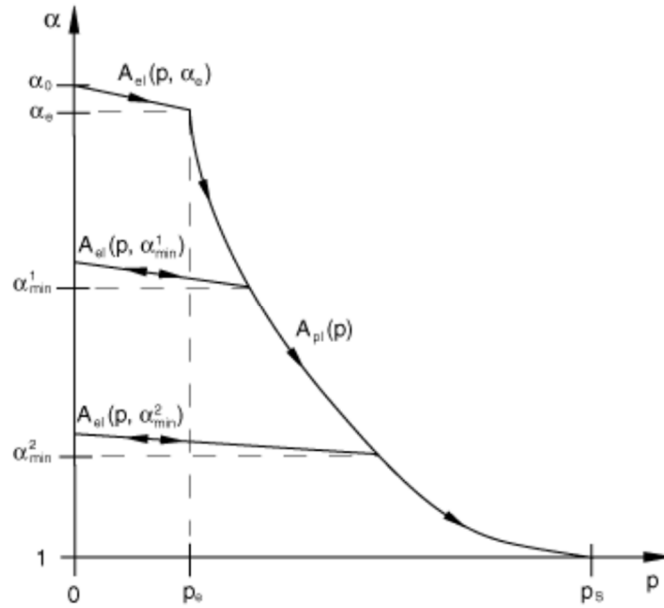
Figure 36 The Compaction Graph of the Ductile Porous Material. [34]

According to Ashby and Gibson, the relationship between the highest possible elastic pressure, the pressure point at which compression becomes irreversible, and the hydrostatic pressure can be expressed in Eqn 10.2. For rigid polyurethane foams, the value of the constant "Cy" is equal to 35 MPa.[35]

$$P_e = \frac{1 - 2v}{1 - v} \sigma_h \tag{10.1}$$

$$\sigma_h = C_y \left(\frac{\rho_0}{\rho_s}\right)^{3/2} + \left(1 + \left(\frac{\rho_0}{\rho_s}\right)^{1/2}\right) \tag{10.2}$$

Another important parameter in the equation used for the plastic compaction curve is n, compaction exponent. D. E. Grady & N. A. Winfree propose the following equation for the compaction exponent of rigid polyurethane material in their work. [36, 37]

$$n = 0.5 + 5.6 \frac{\rho_0}{\rho_s} \tag{11}$$

5.3.2. Shock Equation of State Linear

In this section, we will deal with the exclusively mechanical waves. The mechanical waves are created when a part of a material is moved from its original position and transmits that displacement to adjacent material. Meyer explained the wave at atomic level as the stress transferred from atom to atom at certain specific velocity. In Lattice dynamics the oscillations are coupled with the waves called phonon. In simplified explanation the material even in the static position is continuously vibrating approximately at $\sim 10^{13} s^{-1}$. Phonon waves travel velocity is roughly equal to the velocity of the elastic waves. If we know the interatomic distance, a, of the solid, good approximation can be made. [38]

$$V = \frac{a}{t} \tag{12}$$

However, after that point the material will be assumed as a continuum. Beyond the approximation, the calculation of the elastic wave can be derived with using Newton's second law. In static or quasi-static case, the forces acting on the surface is equal to each other. In case of the impact, material behavior cannot be expressed with static solution, instead dynamic solution needs to be generated. Stress acting on the faces of the infinitesimal rectangular parallelepiped are not equal. Therefore, Newton's second law can be used for the three different axes.

$$F_{x1} = ma_{x1} \tag{13.1}$$

$$F_{x2} = ma_{x2} \tag{13.2}$$

$$F_{x3} = ma_{x3} \tag{13.3}$$

The calculation of elastic wave propagation will be carried out for x_1 axis. Then solution will be extended for other two directions those, x_1 and x_2. The stress acting only in x_1 directions is given (Figure 36).
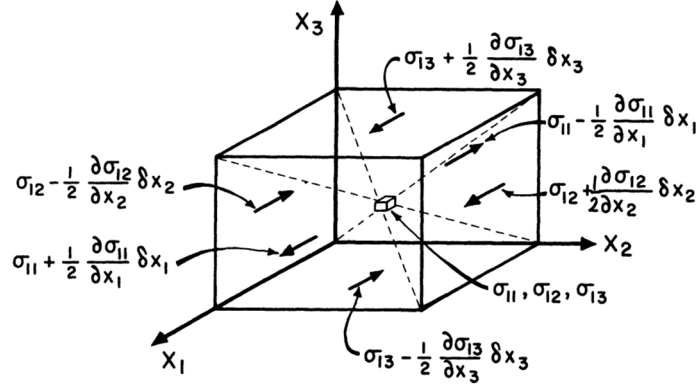
Figure 37 Unit Cube in Dynamic State [37]

The stress acting on each face of the small rectangular parallelepiped is composed of:

$$\sigma_{11} + \frac{\partial \sigma_{11}}{\partial x_1} \cdot \frac{1}{2} \delta x_1 \tag{14.1}$$

$$\sigma_{11} - \frac{\partial \sigma_{11}}{\partial x_1} \cdot \frac{1}{2} \delta x_1 \tag{14.2}$$

$$\sigma_{12} + \frac{\partial \sigma_{12}}{\partial x_2} \cdot \frac{1}{2} \delta x_2 \tag{14.3}$$

$$\sigma_{12} - \frac{\partial \sigma_{12}}{\partial x_2} \cdot \frac{1}{2} \delta x_2 \tag{14.4}$$

$$\sigma_{13} + \frac{\partial \sigma_{13}}{\partial x_3} \cdot \frac{1}{2} \delta x_3 \tag{14.5}$$

$$\sigma_{13} - \frac{\partial \sigma_{13}}{\partial x_3} \cdot \frac{1}{2} \delta x_3 \tag{14.6}$$

In a summary, six separate forces are acting parallel to x_1 axis. In order to find resultant force;

$$\left(\sigma_{11} + \frac{\partial \sigma_{11}}{\partial x_1} \cdot \frac{1}{2} \delta x_1 - \sigma_{11} + \frac{\partial \sigma_{11}}{\partial x_1} \cdot \frac{1}{2} \delta x_1 \right) \delta x_2 \delta x_3$$

$$+ \left(\sigma_{12} + \frac{\partial \sigma_{12}}{\partial x_2} \cdot \frac{1}{2} \delta x_2 - \sigma_{12} + \frac{\partial \sigma_{12}}{\partial x_2} \cdot \frac{1}{2} \delta x_2 \right) \delta x_1 \delta x_3 \tag{15}$$

$$+ \left(\sigma_{13} + \frac{\partial \sigma_{13}}{\partial x_3} \cdot \frac{1}{2} \delta x_3 - \sigma_{13} + \frac{\partial \sigma_{13}}{\partial x_3} \cdot \frac{1}{2} \delta x_3 \right) \delta x_1 \delta x_2 = \sum F_{x_1}$$

After simplification it can be found;

$$\frac{\partial \sigma_{11}}{\partial x_1} + \frac{\partial \sigma_{11}}{\partial x_2} + \frac{\partial \sigma_{11}}{\partial x_3} = \rho \frac{\partial^2 u_1}{\partial t^2} \tag{16.1}$$

For other directions

$$\frac{\partial \sigma_{21}}{\partial x_1} + \frac{\partial \sigma_{22}}{\partial x_2} + \frac{\partial \sigma_{23}}{\partial x_3} = \rho \frac{\partial^2 u_2}{\partial t^2} \tag{16.2}$$

$$\frac{\partial \sigma_{31}}{\partial x_1} + \frac{\partial \sigma_{32}}{\partial x_2} + \frac{\partial \sigma_{33}}{\partial x_3} = \rho \frac{\partial^2 u_3}{\partial t^2} \tag{16.3}$$

As stated in the previous sections, the material exhibits isotropic behavior. For that reason, the formula for Hooke's law that applies to isotropic materials under triaxial stress is utilized. It involves six equations that link the stresses to the strains, where λ, μ represent the Lame constants and Δ dilatation equals to $\varepsilon_{11} + \varepsilon_{22} + \varepsilon_{33}$.

$$\sigma_{11} = \lambda \Delta + 2\mu\varepsilon_{11} \tag{17.1}$$

$$\sigma_{22} = \lambda \Delta + 2\mu\varepsilon_{22} \tag{17.2}$$

$$\sigma_{33} = \lambda \Delta + 2\mu\varepsilon_{33} \tag{17.3}$$

$$\sigma_{12} = 2\mu\varepsilon_{12} \tag{17.4}$$

$$\sigma_{13} = 2\mu\varepsilon_{13} \tag{17.5}$$

$$\sigma_{23} = 2\mu\varepsilon_{23} \tag{17.6}$$

Also, definition of the strain

$$\varepsilon_{11} = \frac{\partial u_1}{\partial x_1} \tag{18.1}$$

$$\varepsilon_{12} = \frac{1}{2}\left(\frac{\partial u_1}{\partial x_2} + \frac{\partial u_2}{\partial x_1}\right) \tag{18.2}$$

$$\varepsilon_{13} = \frac{1}{2}\left(\frac{\partial u_1}{\partial x_3} + \frac{\partial u_3}{\partial x_1}\right) \tag{18.3}$$

By putting the strain expressions, Lame constants, dilatation into the equation and making rearrangement, we could obtain the equations for the propagation of longitudinal and distortional wave

$$(\lambda + \mu)\frac{\partial \Delta}{\partial x_1} + \mu \nabla^2 u_1 = \rho \frac{\partial^2 u_1}{\partial t^2} \qquad (19.1)$$

Likewise, for the x_2 and x_3 directions

$$(\lambda + \mu)\frac{\partial \Delta}{\partial x_2} + \mu \nabla^2 u_2 = \rho \frac{\partial^2 u_2}{\partial t^2} \qquad (19.2)$$

$$(\lambda + \mu)\frac{\partial \Delta}{\partial x_3} + \mu \nabla^2 u_3 = \rho \frac{\partial^2 u_3}{\partial t^2} \qquad (19.3)$$

As a result, if we substitute the displacements in the equations with strains, and then differentiate Eqn. with respect to x_1, x_2, and x_3, we obtain a set of grouped equations

$$\frac{\partial^2 \Delta}{\partial t^2} = \frac{\lambda + 2\mu}{\rho}\nabla^2 \Delta \qquad (20.1)$$

where the operator ∇^2 corresponds to

$$\nabla^2 = \frac{\partial^2}{\partial x_1^2} + \frac{\partial^2}{\partial x_2^2} + \frac{\partial^2}{\partial x_3^2} \qquad (20.2)$$

It can be easily noticed that the general wave equation is similar to this second-order partial differential equation.

$$\frac{\partial^2 y}{\partial t^2} = V^2 \frac{\partial^2 y}{\partial x^2} \qquad (21)$$

Then the dilatational wave, is also commonly known as "bulk sound speed" can be written as [38]

$$V_{long} = \left(\frac{\lambda + 2\mu}{\rho}\right)^{1/2} \qquad (22.1)$$

The Lame constants are often used in the analysis of wave propagation in elastic materials, also used to model the behavior of structures and materials in response to loads and boundary conditions in finite element method.

Lame constants;

$$\mu = G = \frac{E}{2(1+v)} \tag{22.2}$$

$$\lambda = \frac{Ev}{(1+v)(1-2v)} \tag{22.3}$$

Bulk sound of speed can also be written with the parameters ρ, E, v which are density, Young Modulus and Poisson ratio respectively.[38]

$$V_{long} \equiv C_1 = \left[\frac{(1-v)}{(1+v)(1-2v)} \frac{E}{\rho} \right]^{1/2} \tag{22.4}$$

The effort to determine these parameters was explained in Chapter 4 "Material Characterization" section.

To find the distortional (shear) wave velocity, we must eliminate Δ from Eqn. [19.1] by taking its derivative with respect to x_2 and from Eqn. [19.2] with respect to x_1. Finally, shear waves can be written as [38]

$$V_s \equiv C_s = \left(\frac{\mu}{\rho} \right)^{1/2} \tag{23}$$

The relation between Surface (or Rayleigh) waves and shear waves can be approximated by following equation [38]

$$C_R = \frac{0.862 + 1.14v}{1+v} C_S \tag{24}$$

The snow plow shock model refers to a mathematical representation of the impact of a snow plow on the snow cover in front of it as it moves forward. This impact, referred to

as a "shockwave," involves the transfer of mass, momentum, and energy from the snow cover to the plow. The model takes into account the velocity of the plow, the width of the plow blade, and the properties of the snow, and uses the Rankine-Hugoniot conditions to describe the changes in mass, momentum, and energy across the shock front. The preservation of mass, momentum, and energy across the shock front results in three equations known as the Rankine-Hugoniot conditions or equation.

$$\rho_0 U_s = \rho_1 (U_s - U_p) \tag{25.1}$$

$$P_1 - P_0 = \rho_0 U_s U_p \tag{25.2}$$

$$P_1 U_p = \frac{1}{2} \rho_0 U_s U_p{}^2 + \rho_0 U_s (e_1 - e_0) \tag{25.3}$$

Using these three-conversation equation we can get

$$U_s{}^2 = \frac{1}{\rho_0^2} \frac{P_1 - P_0}{V_0 - V_1} \tag{26.1}$$

$$\frac{1}{\rho} = V \tag{26.2}$$

The Hugoniot shock curve gives insight into the alterations in pressure and density, which can be determined by only measuring two parameters: the shock velocity (U_s) and the particle velocity (U_p). The relation between the U_s and U_p has be to be determined experimentally. [15]

$$U_s = C_0 + S_1 U_p + S_2 U_p^2 + \cdots \tag{27}$$

S_1 and S_2 are empirical parameters and C_0 is sound velocity in the material. The study of Hugoniot shocks at Los Alamos National Laboratory involves using advanced experimental techniques and numerical simulations to understand the behavior of materials under extreme pressure and temperature conditions. Los Alamos National Laboratory on Hugoniots shock led to the compilation of shock parameters for numerous materials and gathered this information in the LASL Shock Hugoniot Data Handbook. [15].

Table 7 LASL Hugonoit Data for Polyurethane Rigid Foam

ρ_0	U_s	U_p	P	V	ρ	V/V_0
g/cm^3	km/s	km/s	Gpa	cm^3/g	g/cm^3	
0.145	2.227	1.732	0.561	1.5287	0.654	0.222
0.150	2.259	1.736	0.589	1.5424	0.648	0.232
0.149	2.265	1.738	0.585	1.5658	0.639	0.233
0.147	2.227	1.742	0.569	1.4856	0.673	0.218
0.145	2.242	1.750	0.570	1.5093	0.663	0.219
0.159	2.955	2.214	1.043	1.5732	0.636	0.251
0.159	3.058	2.222	1.082	1.7172	0.582	0.273
0.157	3.008	2.225	1.053	1.6548	0.604	0.260
0.149	2.938	2.230	0.976	1.6173	0.618	0.241
0.202	3.057	2.232	1.379	1.3353	0.749	0.270
0.178	3.748	2.878	1.924	1.3011	0.769	0.232
0.158	3.743	2.880	1.702	1.4602	0.685	0.231
0.160	3.782	2.976	1.800	1.3328	0.750	0.213
0.175	3.657	2.961	1.906	1.0575	0.946	0.185
0.156	3.633	2.964	1.693	1.1437	0.874	0.179
0.159	3.685	2.997	1.758	1.1728	0.853	0.187
0.159	3.612	3.006	1.729	1.0539	0.949	0.168
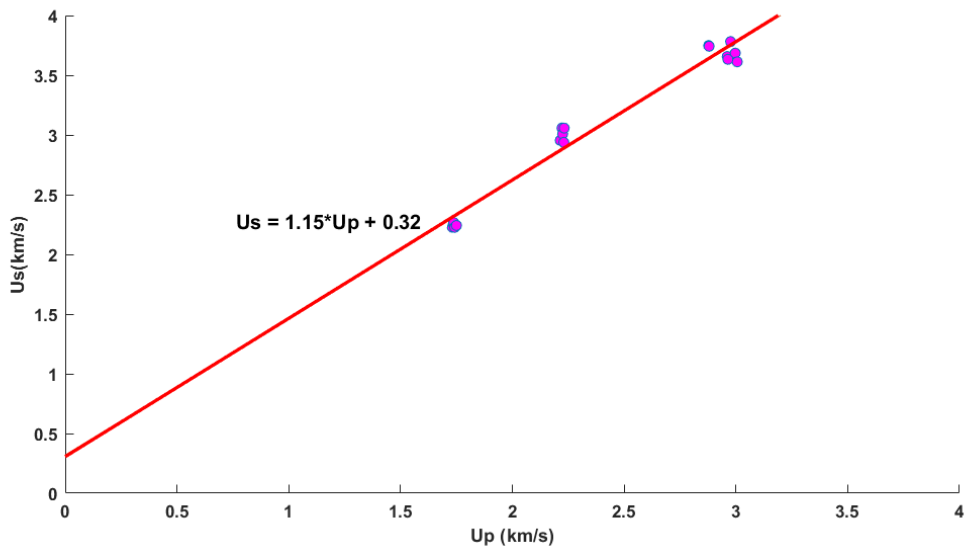
Figure 38 Relation Between Shock velocity vs Particle Velocity [15]

It's noteworthy that the linear equation of state, used to describe the behavior of a material, is not valid when the material has porosity. In such cases, the equation must be modified to accurately reflect the behavior of the system.

The Mie-Grüneisen equation of state (EOS), also known as the Mie-Grüneisen Shock EOS, is an important model in the field of high-strain rate conditions and is particularly

useful for describing the behavior of materials under shock loading and high-speed impact. This EOS is based on statistical mechanics and can be represented using the Grüneisen parameter.

The model accounts for the behavior of both elastic and plastic deformation and is based on the Mie-Grüneisen equation of state. Also, it is used to determine the pressure in a shock-compressed solid and has several variations in use. The Mie-Grüneisen equation is a special form of the Grüneisen model.

A good approximation has been developed by Meyer for Mie- Grüneisen parameter. This relationship is very helpful in providing approximate values for materials that are unknown. [38]

$$\Gamma = 2S_1 - 1 \tag{28}$$

In the previous section, it was mentioned that "K_0" represents the bulk modulus of the solid material. The equation for the bulk sound speed of the material involves the constant "c_0", which corresponds to the bulk sound speed. This equation can be derived using the longitudinal sound speed "V_{long}" and the transverse sound speed "V_s" according to LASL. [39]

$$c = \sqrt{V_L^2 - \frac{4}{3}V_s^2} \tag{29}$$

5.3.3. Engineering Data

Sections 5.3.1 and 5.3.2 provide an explanation of how the parameters for the polyurethane material used in the analysis are obtained through theoretical calculations. Furthermore, section 4.2 includes material characterization studies. The parameters for rigid polyurethane material are presented in a single Table 8.

Table 8 Material Properties of Rigid Polyurethane Needed for Finite Element Analysis

Rigid Polyurethane Properties	
	Value
Shear Modulus	25,06 MPa
Shock Linear EOS	
Gruneissen Coefficient [15]	1,3
Parameter C1[15]	320 m.s^-1
Parameter S1 [15]	1,15
Parameter Quadratic S2 [15]	0 s.m^-1
P-Alpha EOS	
Solid Density [40]	1160 kg.m^-3
Porous Sound of Speed [15]	408,5 m.s^-1
Initial Compaciton Pressure [35]	1,58 MPa
Solid Compaction Pressure [35]	44,99 MPa
Compaction Exponent[36]	1,272

* Material property measured according to international test standards

** Material property measured by reference to the academic study carried out

5.4. Geometry and Model Setup

In order for the design work to begin, the system-level requirements must be clear. The requirements determined at the system level are then broken down into subsystem level requirements. The canister cover should be designed to meet these requirements.

Considering that the canister protects the missile from environmental influences, in many applications, the canister is designed according to the gas-tightness requirements of the cap. To explain this in more detail, the canister cover should be designed to prevent the inlet and outlet of toxic gases, water, and moisture.

EMI stands for Electromagnetic Interference, which refers to the disruption of electronic devices caused by electromagnetic waves. EMI protection refers to the measures taken to prevent or reduce this interference, such as shielding the electronic device with a conductive material or filtering out unwanted electromagnetic frequencies. EMI protection is particularly important in aviation and aerospace systems, and military communications.

Also, the canister's front cover is directly exposed to the exhaust gases of the rocket engine that has been fired by the adjacent canister. That is the main reason for the dome-shaped design, which helps to reduce the effect of external loads.

Due to the weight constraints of military projects, cover design should be carried out using a lightweight design approach that doesn't sacrifice system performance, strength, and durability. The 3D model used in the analysis study is given in Figure 38, giving a general view of the system. To expedite the analysis, design details that were not expected to significantly impact the results were omitted. These included EMI/EMC gasket channels, bolt connection interfaces, small faces, chamfers, and radii.
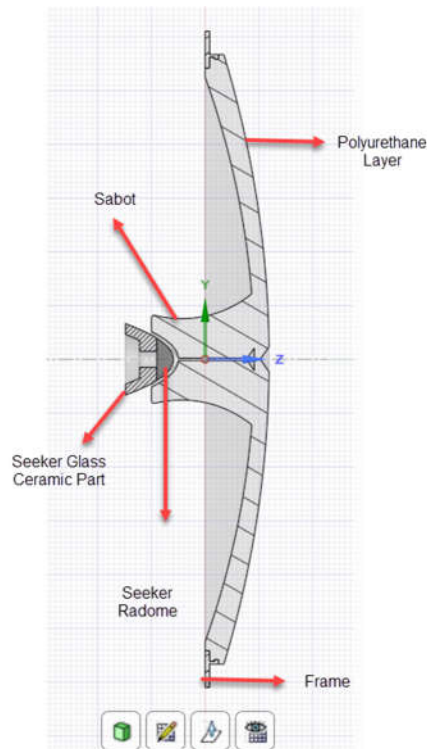
Figure 39 Geometry Used for Finite Element Analysis

Two diagonal notches have been made on the developed canister cover, intersecting at the center. The aim is for the cover to start breaking over this resistively weakened area, and to break along the notch to prevent the cover from splitting into multiple parts.

Additionally, the missile is intended to collide with the cover in a controlled manner. Therefore, sabots have been added to the canister covers. The sabots reduce the distance between the missile and the cover, preventing the missile from gaining momentum before the collision. The sabots are designed as four parts with cushioning and damping properties due to the foam material.

The sabots are positioned on the polyurethane layer to distribute the load equally to the four parts of the cover separated by notches. A space is positioned between the sabot parts so that the sabots, which will be subjected to axial compression with the radome contact, can expand up to certain point in the radial direction. Another factor in the partial positioning of the sabots is that, in case of an unexpected error, the sabot will be attached to the missile radome and fly with the missile for a while. This will directly affect the aerodynamic characteristics and flight performance of the missile.
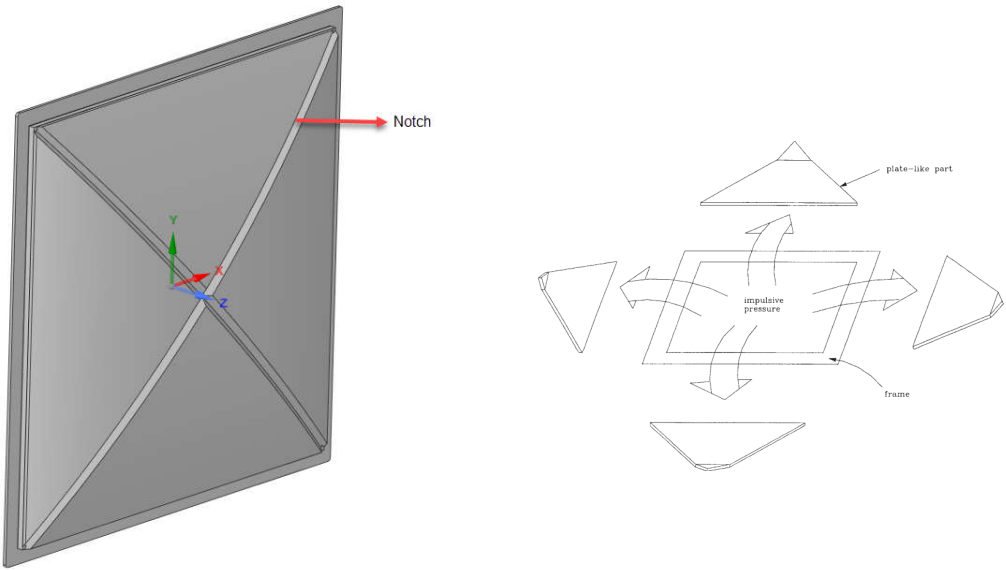
Figure 40 Notches Crossed at the Center of the Cover (Left), Separation of the Parts in Pre-Determined Direction [14]

Stress concentration refers to a localized area on a material or structure where stress is significantly higher than the average stress on the rest of the material. This can occur due

to a change in the shape, size, or geometry of the material, which leads to the stress becoming more concentrated in that particular region.

Stress concentrations are a common concern in engineering and design, as they can significantly affect the strength, durability, and safety of a material or structure. A notch is a V-shaped indentation, typically at the surface of a material, where the material is abruptly reduced in size. when a notch is present, the distribution of stress is altered, and the stress becomes concentrated at the base of the notch. Shortly, the notches causes to stress concentration.

It is aimed that the notch on the canister cover is subject to tension with internal loading and compression with external loading. Thus, while it will be broken more easily with internal loading, it will be more difficult to break with external loading. The notch depth and width are seen in Figure 40.
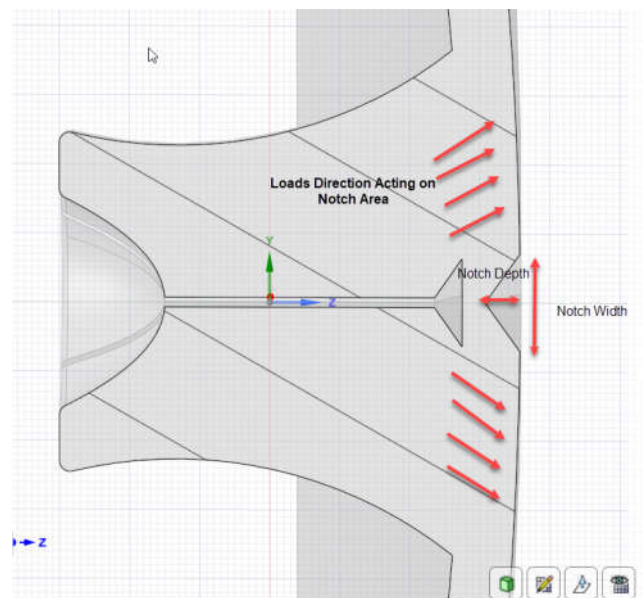
Figure 41 Notch Depth vs Notch Width

Therefore, local mesh control is applied to the notched surfaces to obtain a more precise result. Face sizing is a mesh control technique that allows for the specification of a target size for the mesh elements on a specific face or set of faces. As a result, the notched

surfaces were subjected to the face sizing method to refine the mesh elements and improve the accuracy of the simulation

Sphere of influence mesh control is a technique used in mesh generation, where the mesh is refined around specific areas of interest, known as the sphere of influence. This technique helps to improve the accuracy of simulations by increasing the mesh density in regions where high resolution is required, while keeping the mesh density low in other areas to reduce computational costs.
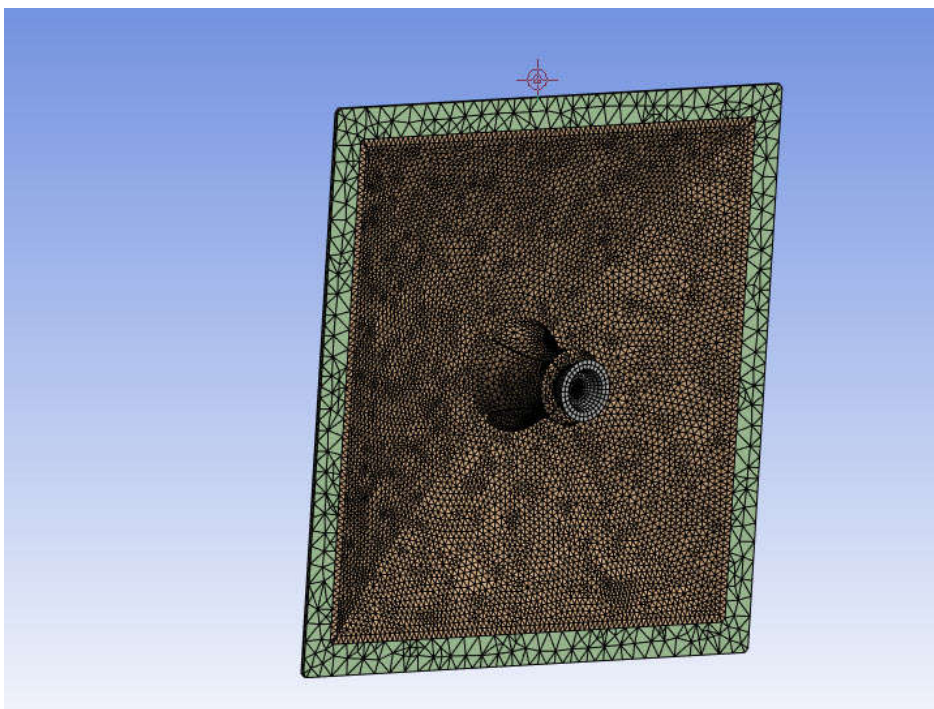
Figure 42 View of Mesh Structure

Aspect ratio is a mesh quality metric commonly used in explicit analysis to evaluate the quality of the mesh elements. It is defined as the ratio of the longest edge of an element to the shortest edge. A high aspect ratio indicates that an element is highly distorted, which can lead to inaccuracies in the simulation results.

In explicit analysis, it is important to have a high-quality mesh with elements that have low aspect ratios. This is because high aspect ratios can cause elements to fail or even

break apart during simulation, leading to incorrect results. Therefore, aspect ratio is an important factor to consider when creating and evaluating meshes for explicit analysis.
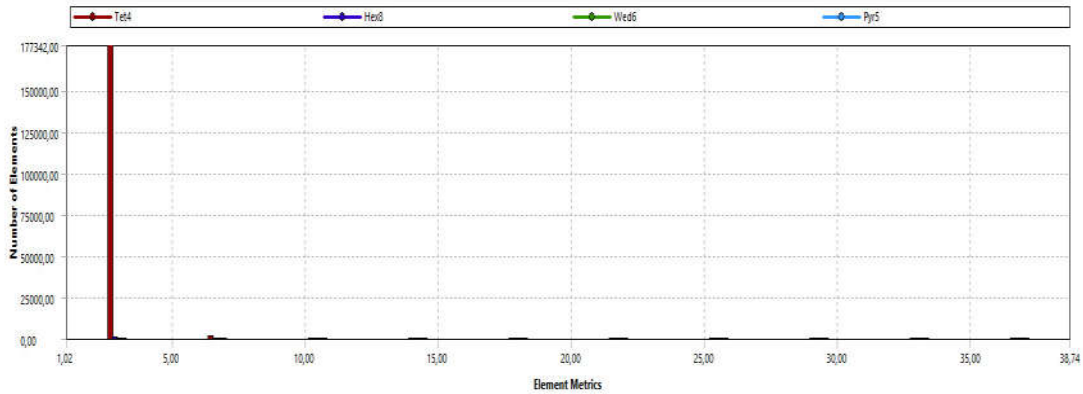
Figure 43 Mesh Quality Metric- Aspect Ratio

The use of point masses can simplify the finite element analysis by reducing the size and complexity of the model, while still accurately representing the behavior of the structure. missile's inertia, center of gravity and center of mass information are well defined. Also, most of the missile will not interacted with canister cover. In this context, it is appropriate to use a point mass for the remaining mass while modeling some of the radome and seeker parts.

Remote displacement is a technique used in ANSYS analysis to constrain the degrees of freedom of a model. For the purposes of the analysis, it is assumed that the missile moves along a single axis, while its movement in the remaining two axes and directions of rotation are constrained. The remote displacement boundary condition was applied to a reference surface that is rigid and does not deform under the applied loads.

5.5. Analysis Results

Within this section, users have the option to choose and view various outcomes, including deformations, stresses, strains, energies, and reaction forces, among others. These

outcomes will be thoroughly explained. Specifically, for this examination, our focus is on the reaction forces and deformation.

5.5.1. Deformation

To evenly distribute the load to four sections of the cover the sabots are placed on polyurethane layer. To allow for expansion in the radial direction, there is space between the sabot parts which will undergo axial compression when in contact with the radome. After a certain point, the sabots come into contact with each other. And this contact creates a radial force.
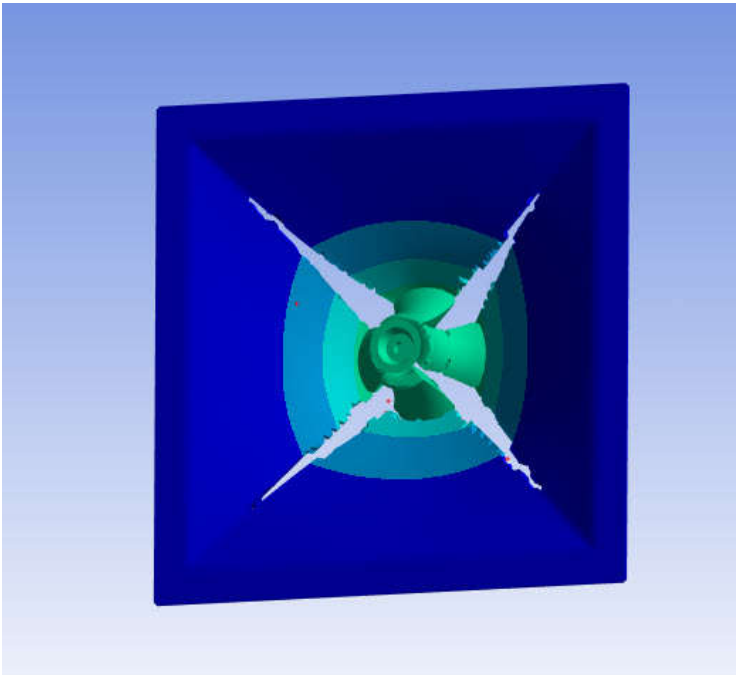
Figure 44 Breaking Four Parts due to Radial and Axial Loading

The notches in the cover become exposed tension due to movement of the missile in axial direction. The canister cover subjected to these loading starts breaking at the intersection of the notches. At the same time the canister cover parts move away from the trajectory of the missile due to the load created with the contact of the sabots to each other.
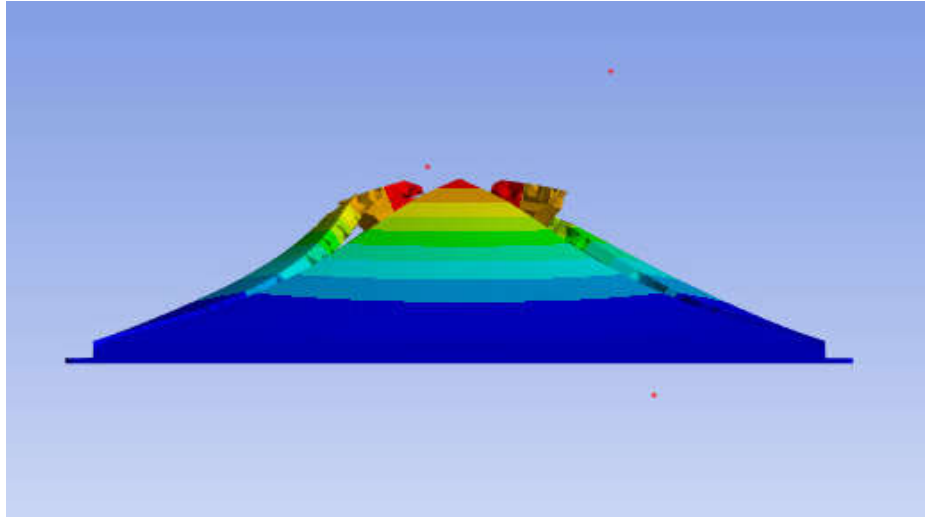
Figure 45 The Notches Exposed to the Tension

Principal strain limit failure is a type of failure criterion used in ANSYS Mechanical to predict the failure of a material under mechanical loading. It is based on the concept of principal strains, which are the maximum and minimum strains experienced by a material in a given loading scenario. The principal strain limit failure criterion is typically used for ductile materials such as metals, which tend to deform significantly before failing.
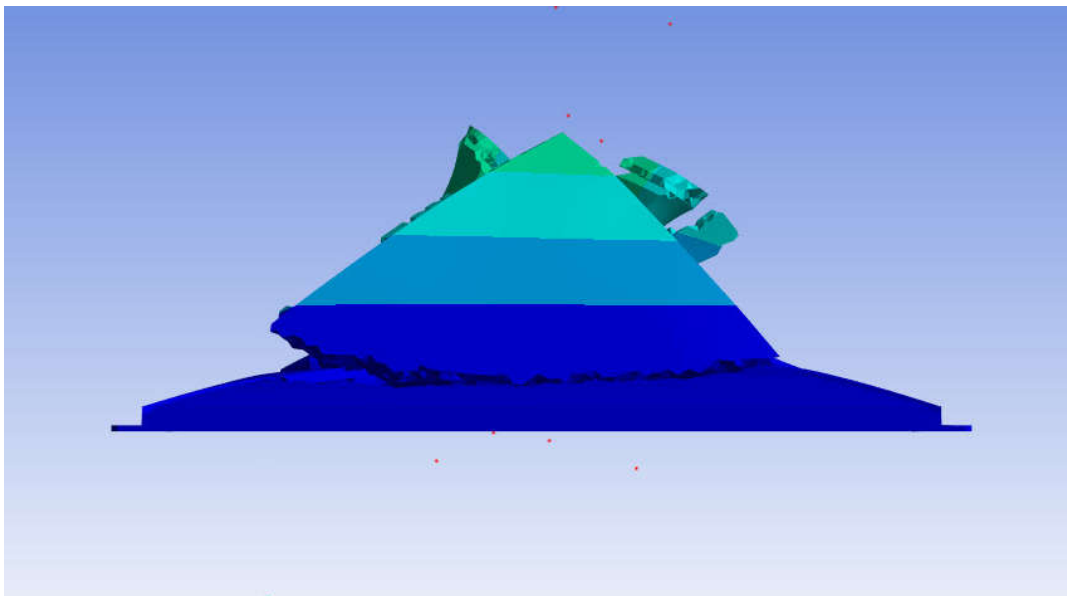
Figure 46 Failure of the Canister Cover.

The principal strain limit failure criterion predicts failure based on the maximum principal strain or the difference between the maximum and minimum principal strains. If it

exceeds a certain limit, the material is predicted to fail. It's important to note that failure criteria like principal strain limit are only predictions, and real-world materials may exhibit more complex behavior. Therefore, it's always important to validate simulation results against experimental.

The breaking sequence of the sabot parts and cover layers destabilizes the radial forces acting on the missile radome tip. This causes the missile to deviate from its trajectory. The combination of thrust misalignment of the missile and radial loads due to breakage reduces system accuracy.
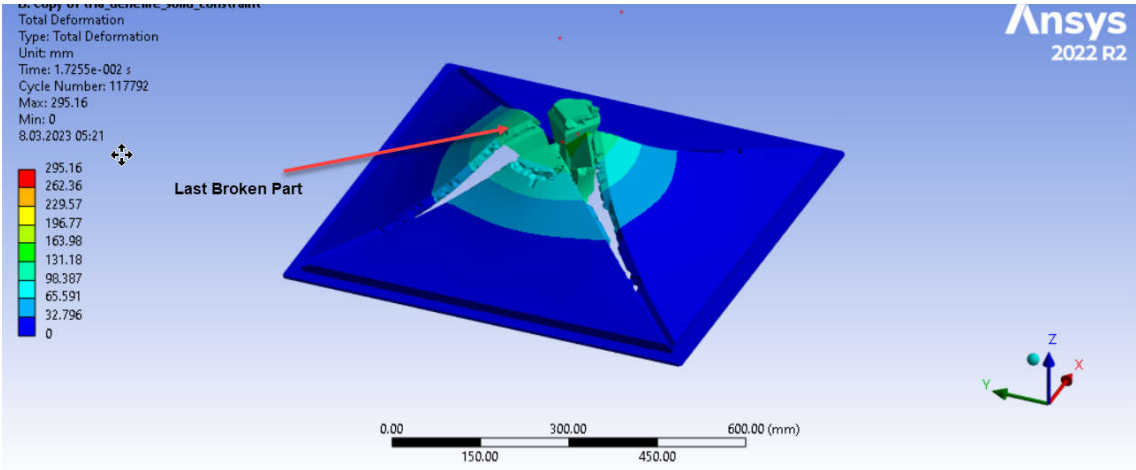
Figure 47 The Piece that Broke Last, Causing Displacement in the Y Direction

In the analysis performed without considering missile shoe and launching rail interaction it was seen that the impact caused missile a 25 mm displacement in the y direction. For reduce tip-off effect during launch, dynamic modeling of missile shoe placement and missile launch rail interaction is required.
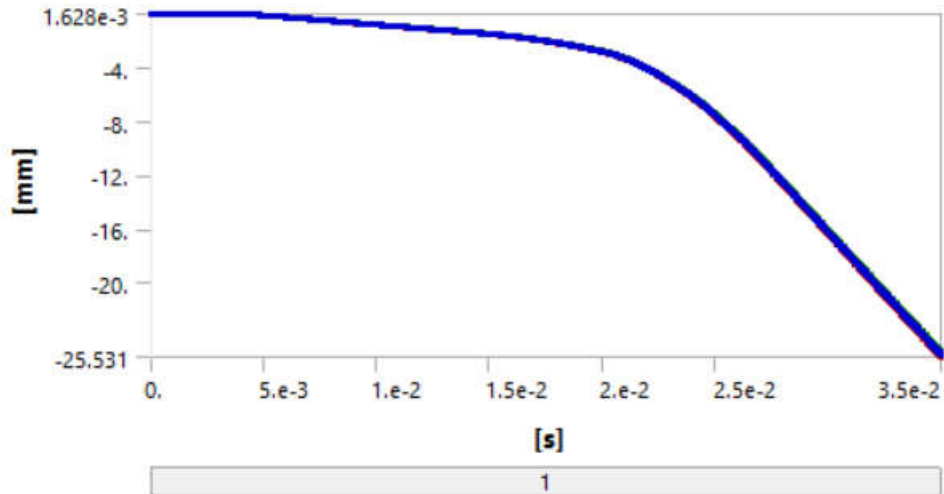
Figure 48 Displacement of Radome and Seeker in Y Direction

The graph of the displacement of the missile in the x direction without considering missile shoe and launching rail interaction is given below. The output from these graphs provides information on where the missile shoe should be placed in the structural body.
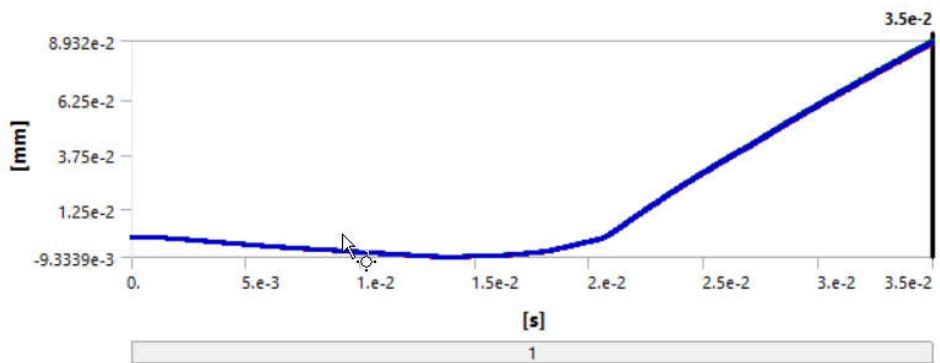
Figure 49 Displacement of Radome and Ceramic Seeker in X Direction

FEA is used to simulate the behavior of structures and systems under different conditions. The accuracy of these simulations is critical to making informed decisions about the design and performance of these structures and systems. Validating FEA models helps ensure that the simulations accurately reflect the behavior of the real-world system being modeled.

Figure 50 Validation of Simulation

5.5.2. Force Acting on Ceramic Seeker.

Bonded and frictionless contact models are two types of contact algorithms used in explicit analysis to simulate contact between bodies. The main difference between the two models is how they handle tangential forces at the contact interface.

In a bonded contact model, the two bodies are assumed to stick together and move as a single body when in contact. The contact interface is modeled as perfectly bonded, and there is no relative motion allowed between the two bodies in the tangential direction. Therefore, there is no sliding or frictional force at the contact interface. This type of contact model is appropriate for simulating interfaces where there is a strong bonding between the two bodies, such as in adhesive bonding or welding.

In a frictionless contact model, the two bodies are assumed to slide against each other at the contact interface without any resistance. The normal force acting perpendicular to the contact surface is calculated based on the overlap of the two bodies, while the tangential force is calculated based on the relative velocity of the two bodies at the contact interface.

However, there is no frictional force between the two bodies in the tangential direction. This type of contact model is appropriate for simulating interfaces where there is little or no friction between the two bodies, such as in some types of impact or collision scenarios.
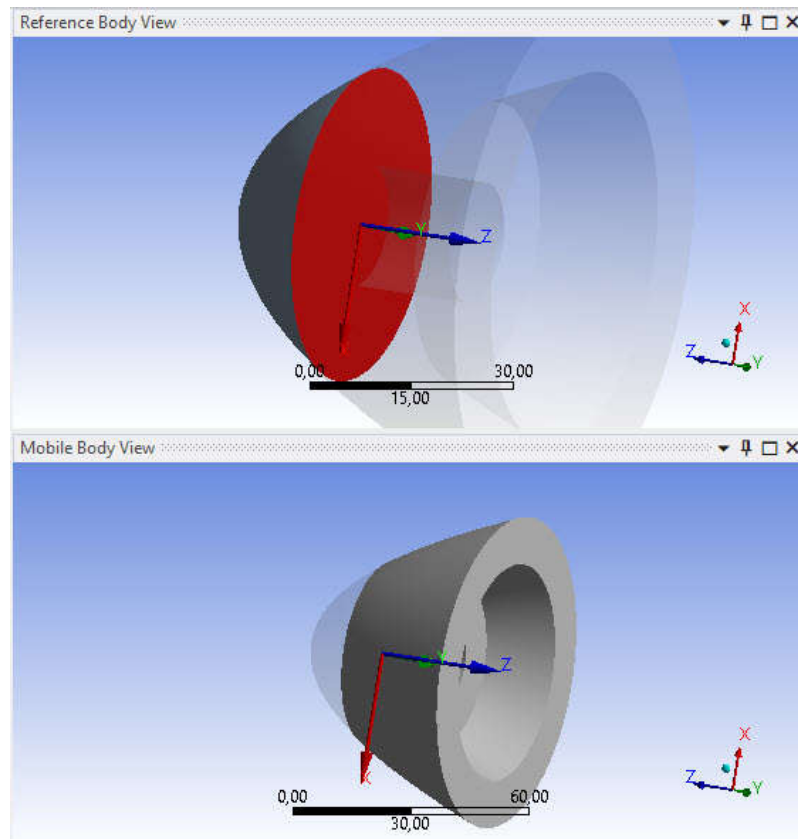
Figure 51 Radome and Ceramic Seeker Contact

The missile's random is made of a high-strength metal material, which makes it rigid. To ensure the reliability of the structural analysis studies that will be conducted using the force applied to the ceramic seeker, the transfer is done without damping.

A joint that allows the user to measure forces at the interface between Radome and Ceramic Seeker. The joint probe in ANSYS allows the user to measure a wide range of quantities, including reaction forces, moments, contact pressures, and contact stresses. These quantities can be measured in different directions and at different locations along the interface.
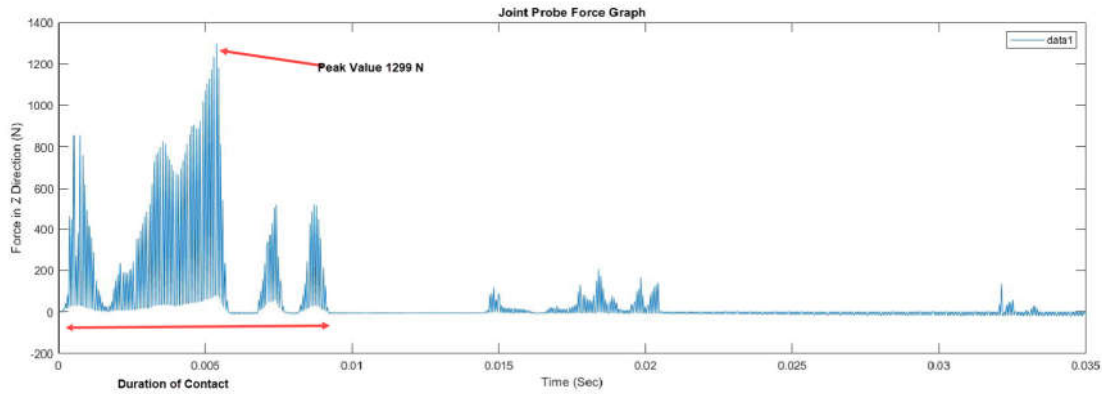
Figure 52 Force Acting on Ceramic Seeker
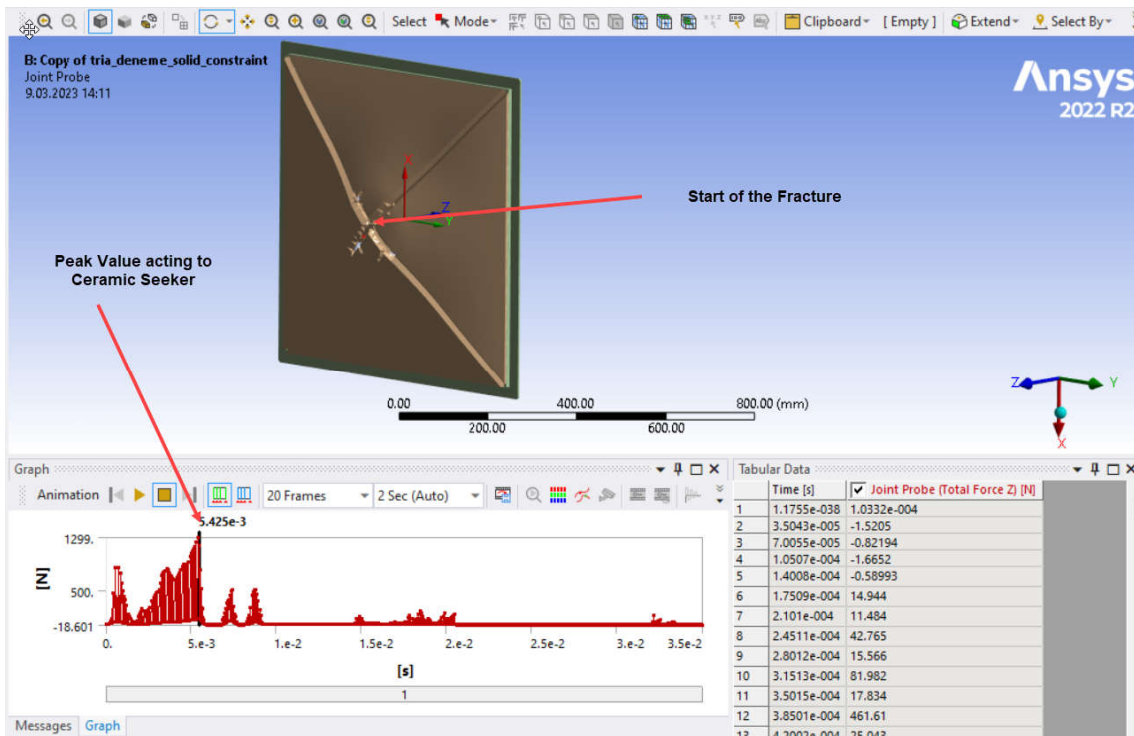
Figure 53 Maximum Force Acting Ceramic Seeker and Start of the Fracture

The results indicate that the ceramic seeker experienced the highest force transfer when the canister cover began to fracture, as illustrated in Figure 52. The corresponding force acting on the ceramic seeker is shown in Figure 51 and was found to reach a maximum value of 1299 N. Based on the data, it can be observed that fracture of the canister cover was completed approximately within 90 milliseconds. The small peaks located on the right side of the graph can be attributed to the contact between the radome and the broken fragments following the fracture event.
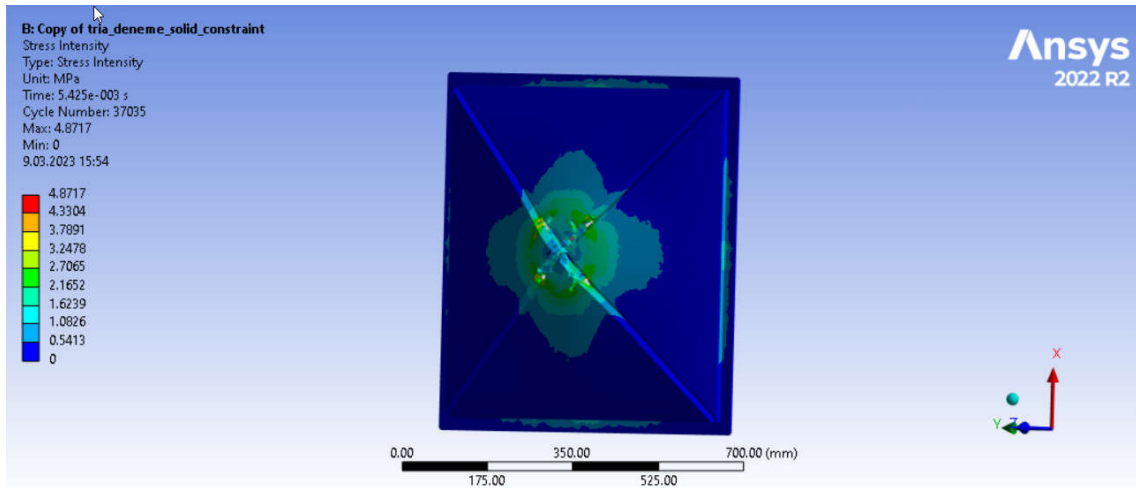
Figure 54 Stress Intensity Factor

To ensure the canister cover meets the required specifications for its life cycle, it must meet numerous requirements. However, in accordance with the current study, minimizing the force acting on the ceramic seeker was selected as the primary success criterion. To achieve this goal, notches were incorporated into the design of the canister cover. As stated previously, the notch effect and stress intensity are two important concepts in the field of fracture mechanics. The notch effect refers to the phenomenon where the presence of a notch or a crack in a material can significantly reduce its resistance to fracture. As shown in Figure 53, the stress intensity factor observed on the cover when the ceramic seeker was subjected to the maximum load was 4.817.

6. TEST

6.1. Test Setup

Product validation testing is a type of testing that is performed to ensure that a product meets the needs and expectations of its target. The ultimate goal of product validation testing is to provide confidence that the product will meet the system requirement and expectations of the end user, and that it is fit for its intended purpose.

For this reason, it is necessary to design a test stand that will ensure the contact of the radome and the cover with the speed specified in section 3.1.2. It is a challenging task to design a test stand that will simulate the trust force resulting from the thermochemical reaction that takes place inside the missile engine. In the literature search, only one test stand was encountered. In the study carried out by Jae-Wook Chung, et al, 2013, conservation of kinetic energy was aimed. The hydraulic circuit diagram of the test stand is given in Figure 49. [12]
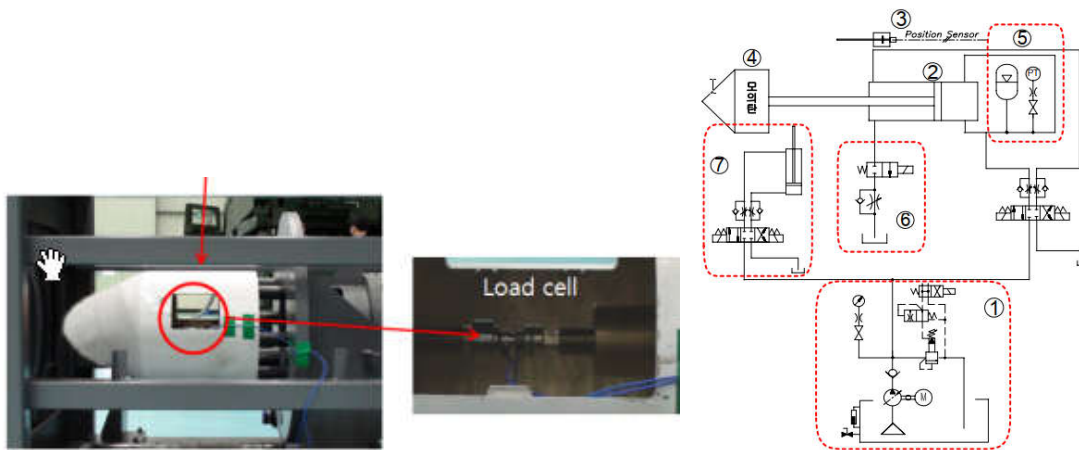
Figure 55 Overview of the Test Bench (Left), Hydraulic Circuit Diagram of the Test Bench [12]

Verifying the fragile canister cover through firing test activities presents several significant obstacles, including high costs, extensive manpower requirements, and non-repeatability of tests. In light of these challenges, it was determined that ground tests would be a more effective approach.

The test stand was designed with the fiction that the collision speed, in other words, the kinetic energy is the same as the real system. More distance is needed to reach target speed because a similar thrust profile cannot be created. It was decided to be designed a pneumatically driven system.
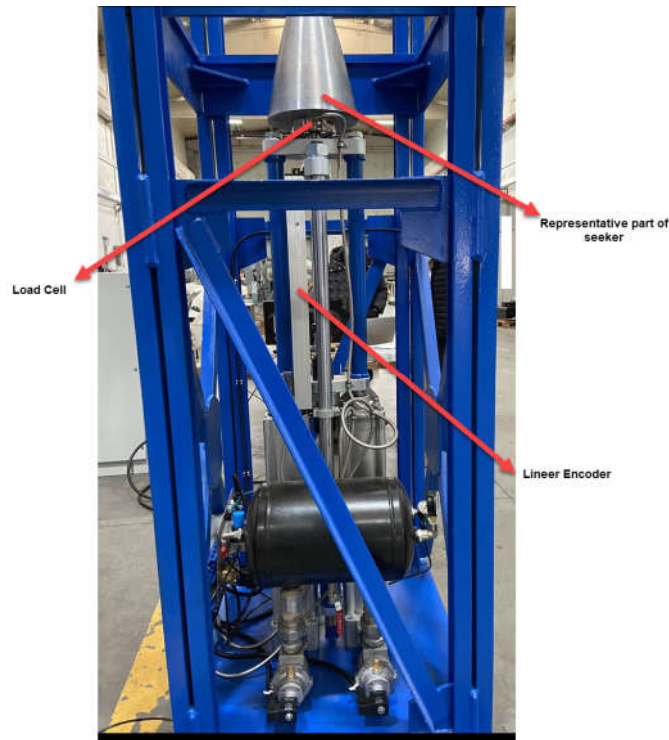
Figure 56 Overview of the Test Bench Used for Validation

The graphical user interface (GUI) developed in Java programming language establishes communication with a programmable logic controller (PLC) to control the test stand. The pressure sensor installed on the tank verifies if the target pressure for the test has been reached, and if the pressure exceeds the intended value, the excess air is released through the relief valve. The gas needed for piston movement is supplied from the tank to the piston through pulse solenoid valves, ensuring a quick and precise delivery. During piston movement, the linear encoder records the displacement measurement, while the load cell data is collected to assess the load transferred to the seeker during the impact. The position of the piston in the zero position is determined by a mechanical limit switch to establish the distance between the seeker and the canister cover. To conduct repeated tests, the previous gas in the cylinder needs to be evacuated, which is done through a relief valve

installed at the entrance of the piston cylinders in addition to the relief valve on the tank. The schematic view of the test stand is presented in Figure 56.
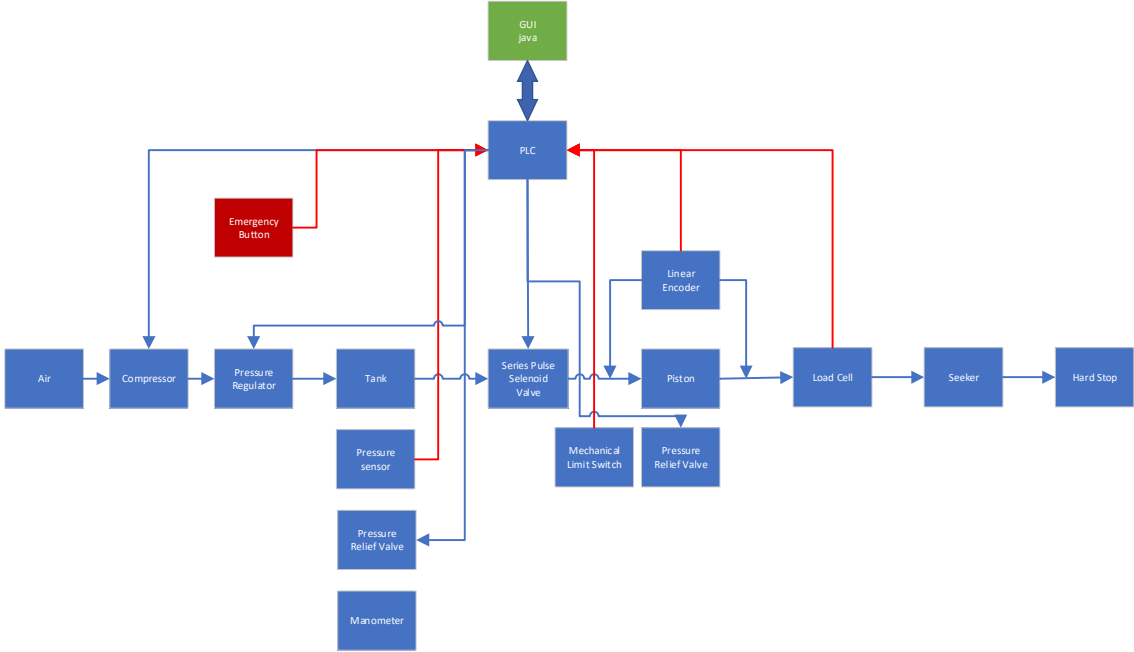
Figure 57 Schematic View of the Test Setup Components

6.2. Test Results

Data is collected with the load cell and linear encoder on the test stand. In addition, fast camera systems were used to monitor the breaking behavior of the designed cover. Image processing was carried out with the stickers attached to the part used instead of the seeker structure. The velocity data obtained from camera recordings and the linear encoder were compared.
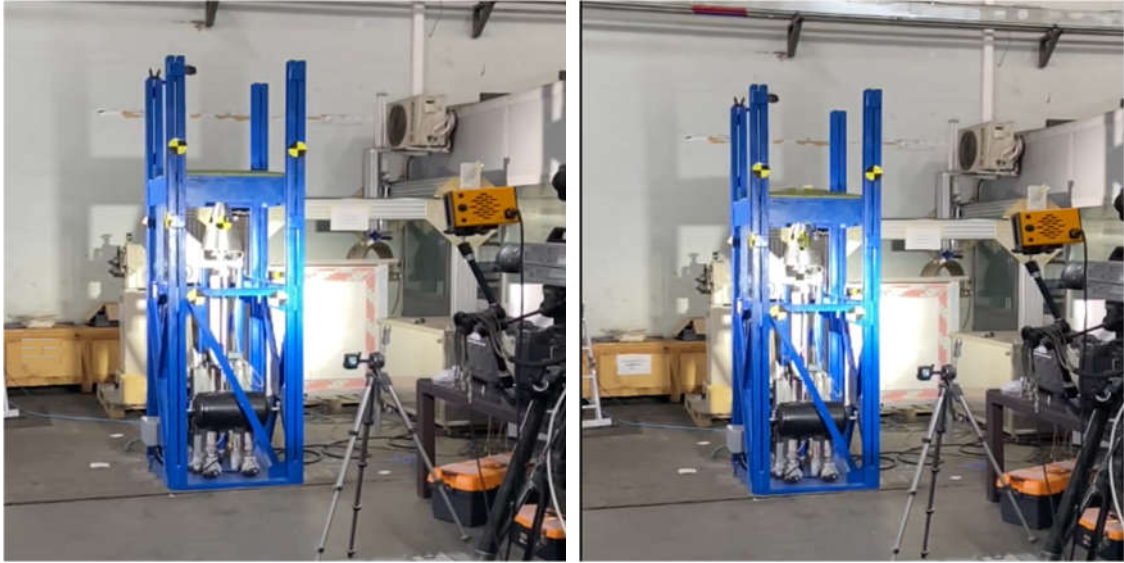
Figure 58 The Static Position of the Test Stand and just Before It Comes into Contact with the Cover
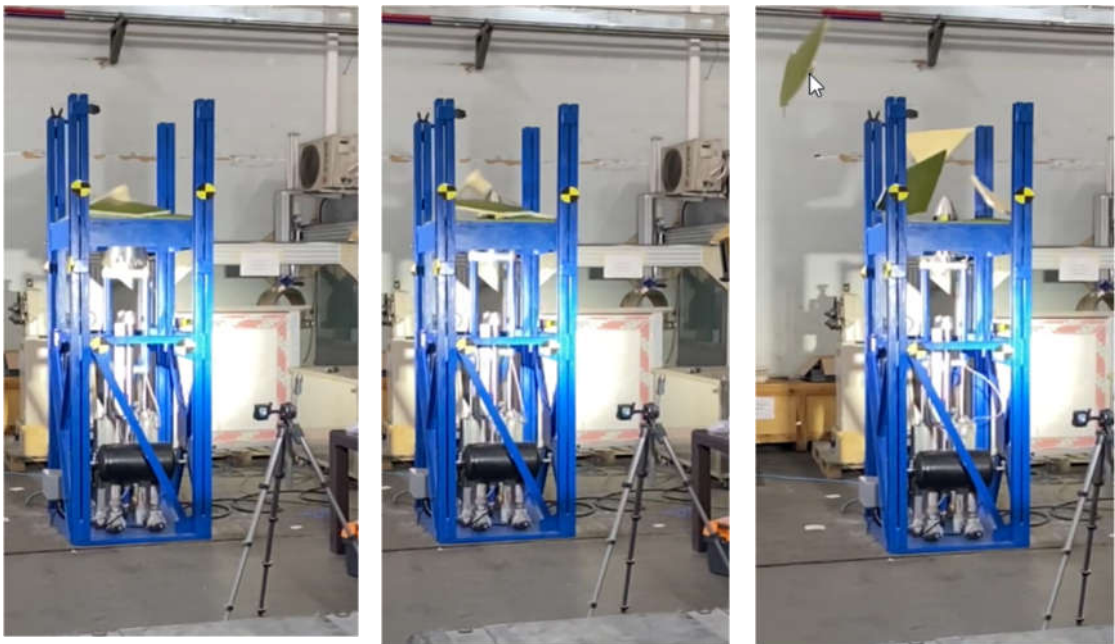
Figure 59 Fractured in Four Parts and Move Away from the Missile Trajectory
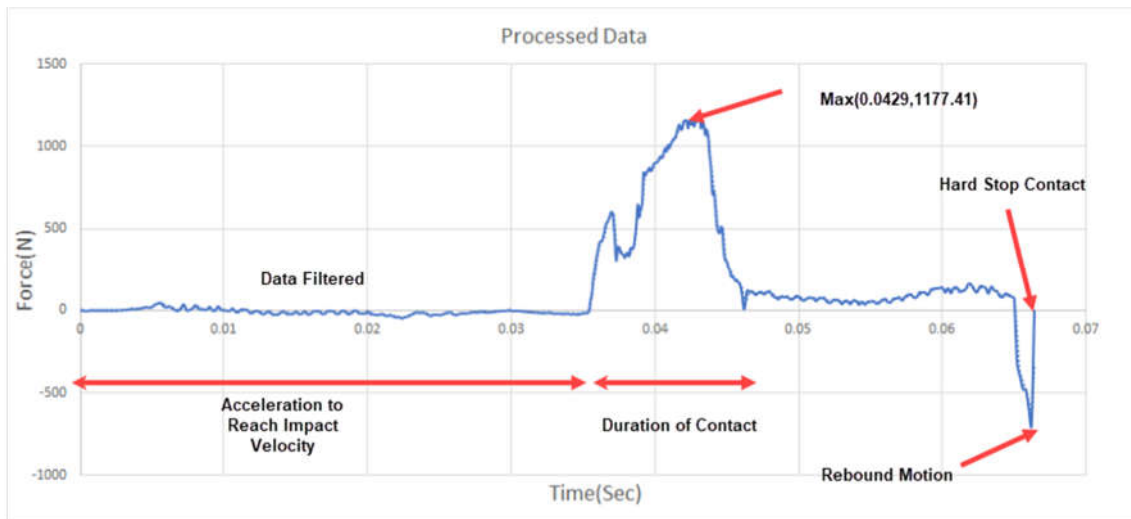
Figure 60 Force Acting on Ceramic Seeker vs Time Recorded by Test Setup

In order to minimize time and effort, the missile radome and canister cover are positioned at the closest possible distance in finite element analysis. As outlined in Section 3.1.2. to determine the impact velocity generated by the rocket engine at a specific displacement the calculation was carried out.

The test setup cannot provide the same thrust force at the same displacement as the rocket engine. The missile nose makes contact in 35 ms, and the duration of contact is approximately 110 ms, as depicted in Figure 58. The pistons in the test setup are equipped with hard stops coated with rubber material to ensure safe stoppage when they reach their displacement limits. The graph's right section represents the rebound movement after the impact.

Peak force value in analysis is higher approximately 9.3% than the force recorded by the test setup. The primary cause for this phenomenon is attributed to the rigid modeling of the radome and ceramic seeker components This modeling approach has resulted in an overestimation of the amplitude force. Furthermore, the elevated magnitude of the load value acquired from the simulation has facilitated adherence to a safe range within the structural analysis investigations being undertaken. To verify the accuracy of the analysis, the acquired experimental data was compared to the results of the simulation, yielding a well-correlated outcome.

7. DISCUSSION AND CONCLUSION

7.1. Discussion

The Section 2.1 describes the various types of canister covers used in missile launch tubes, including electromechanical driven covers, mechanism-activated covers, canister covers ruptured by blast effect, covers broken by random impact, and pyrotechnic-containing canister covers.

In Section 2.2, The literature search reviewed studies related to the design and production of canister covers used in missiles. It is important to note that the lack of academic studies in the areas of foam material impact modeling, canister cover finite element analysis, validation of canister cover compliance with requirements, and material characterization tests may have significant implications for the practical application and safety of these materials and components.

Therefore, the aim of this thesis study is to address these deficiencies in the literature by conducting a comprehensive investigation into each of these areas. Through this study, it is hoped that a greater understanding of these materials and components can be achieved, which may ultimately contribute to the development of more effective and safe engineering practice.

The section 3 discusses the loads that affect the canister cover after engine ignition, which can be classified into three categories: air-blast effect, radome impact, and exhaust gas effect. The effect of the exhaust gases is not considered in this study because a collision occurs between the missile radome and the cover, before the exhaust gases' dynamic effect reaches the front cover. The loads to be used within the scope of the analyses to be carried out must be calculated, created by the analysis method or obtained by the test method. Therefore, it is crucial to use accurate and reliable parameters for these tests, including the type and placement of sensors, the measurement frequency, and the filter used.

The section 4.1 describes the use of rigid polyurethane in various industries such as construction, automotive, and clothing, where a mixture of isocyanate, polyol, blowing agents, and catalyst is pressurized and poured into a die for curing in less than an hour. The cellular structure of the foam affects its mechanical properties, with closed cell foams being more rigid and open cell foams being more flexible. The cellular morphology of the foam can be examined using scanning electron microscopy. The production process of the polyurethane casting mold, including the design and production of the aluminum mold, has been carried out, and trial productions have been done to determine the mold's heating, separation methodology, pressure, and curing time.

In section 4.2, the characterization tests that were carried out to determine the properties of the rigid polyurethane material used in the study was reported. Although the material showed viscoelastic behavior, the dynamic mechanical analysis test could not be performed. Although many characterization tests were performed, the data to be used in the analysis study, which included uniaxial tensile and compression tests, density, durometer hardness, and fracture toughness were given in thesis.

Section 5.1 and 5.2 discusses the use of finite element analysis to investigate the mechanical behavior of canister covers under different loads. The study utilized the Ansys FEM software to perform numerical simulations of the impact scenarios Explicit time integration methods were chosen for this study due to their effectiveness in solving engineering problems with short-duration forces, such as impact, penetration, crash, shock wave propagation, buckling, and instantaneous material failure

The explicit dynamics solution was selected for this study due to the large deformation and strain of canister covers with contact of missile radome, nonlinear material behavior of the foam material, failure, fragmentation, and complex contact between radome and canister cover.

In section 5.3 The P-α compaction model is expressed. This compaction model is used to describe the behavior of ductile porous materials under stress and compression. The P-α

equation of state assumes that when a stress is applied to a porous material, it will first respond elastically, and as the stress increases, the pores in the material will eventually be crushed, resulting in plastic compression that cannot be reversed. This behavior can be modeled using the P-α equation of state, which relates the pressure of the porous material to the scalar variable α, which represents the ratio of the density of solid material to the density of the porous material.

To address this issue, a shock equation of state can be used to model the behavior of the material under shock conditions. The shock equation of state provides a simplified relationship between the pressure, density, and internal energy of the material during shock wave propagation, which can be incorporated into the compaction model. This approach reduces the computational cost and complexity of the analysis while still providing an accurate representation of the material behavior under shock conditions.

The section 5.5. discusses the various outcomes including deformations, stresses, strains, and reaction forces. The focus of the examination is on the reaction forces and deformation. To distribute the load evenly to four sections of the cover, sabots are placed on a polyurethane layer, and space is provided between the sabot parts to allow for expansion in the radial direction. The notches in the cover become exposed to tension due to movement of the missile in the axial direction, and the canister cover subjected to these loading starts breaking at the intersection of the notches. The principal strain limit failure criterion is used in ANSYS Mechanical to predict the failure of a material under mechanical loading.

In Section 6 it is explained that product validation testing ensures that a product meets the needs and expectations of its target users and is fit for its intended purpose. A test stand must be designed to ensure that the product meets system requirements and user expectations. Designing a test stand that simulates the thermochemical reaction inside a missile engine is challenging, but one study aimed to conserve kinetic energy. The test stand was designed to reach the collision speed and kinetic energy of the real system using a pneumatically driven system.

7.2. Conclusion

To improve the accuracy of the shock equation of state, future works should focus on calibrating its parameters based on experimental data or numerical simulations of shock compression experiments. Without this calibration, the shock equation of state may not capture the behavior of the material under high-pressure and high-strain rate loading conditions with precision. In addition, given the difficulty of pressurizing the canister cover to air blast pressure level, further studies should be conducted to simulate the air blast effect and validate the results. Furthermore, it is important to repeat the tests with the cover in its final configuration to ensure that the test results accurately reflect the behavior of the cover under real-world conditions.

In conclusion, this thesis aimed to address the lack of academic studies in key areas related to the design and production of canister covers used in missiles. The literature search revealed significant gaps in foam material impact modeling, canister cover finite element analysis, validation of canister cover compliance with requirements, and material characterization tests. Through a comprehensive investigation of each of these areas, this study has contributed to a greater understanding of the behavior of these materials and components under high-pressure and high-strain rate loading conditions. The results of the tests and numerical simulations carried out in this study have provided valuable insights into the behavior of the canister cover under various loading conditions. Additionally, the design and development of a test stand for product validation testing have demonstrated the importance of this type of testing in ensuring that the product meets the needs and expectations of its target users.

8. REFERENCES

1. Latest military technology shown off at exhibition (2015) YouTube. YouTube.
   Available at:
   https://www.youtube.com/watch?v=0eDNW52eAGQ&ab_channel=APArchive
   (Accessed: March 23, 2023).

2. Larson, L.R. et al., Concentric Canister Launcher., U.S. Patent No. 6,230,604 B1,
   2001

3. Naval strike missile NSM JSM kongsberg defence. Available at:
   https://www.seaforces.org/wpnsys/SURFACE/KDS-Naval-Strike-Missile.htm
   (Accessed: February 22, 2023).

4. Zhang, C. et al., A Novel Non-separation Opening Scheme of Front Cover for
   Rocket Launch Canister, Defence Technology, 15(6), pp. 905–911, **2019**

5. Glass ceramics: Glass Ceramics, Macor, and Corning Pyroceram | Corning.
   Available at: https://www.corning.com/worldwide/en/products/advanced-
   optics/product-materials/specialty-glass-and-glass-ceramics/glass-ceramics.html
   (Accessed: February 22, 2023).

6. Lee, C., Kim, I. S., and Lee, B., Slow crack growth in a cordierite-based glass–
   ceramic missile radome due to stress corrosion, Engineering Failure Analysis, 93,
   76–86, **2018**

7. RIM-7 sea sparrow Wikipedia. Wikimedia Foundation. Available at:
   https://en.wikipedia.org/wiki/RIM-7_Sea_Sparrow (Accessed: February 22,
   2023).

8. Interbartolo, M., Apollo Spacecraft & Saturn V Launch Vehicle Pyrotechnics /
   Explosive Devices, NASA Technical Reports Server (NTRS). Available at:

https://ntrs.nasa.gov/api/citations/20090015395/downloads/20090015395.pdf
(Accessed: February 21, 2023).

9. Choi, W., and Jung, S., Launch Performance Degradation of the Rupture-type Missile Canister, Applied Sciences (Switzerland), 9(7), **2019**

10. Adeel, K.M., Finite element analysis of sandwich structures with viscoelastic foam cores for mechanical applications. Master of Thesis. Politecnico Di Torino, **2019**

11. Akkaş, O., DESIGN OF A FRANGIBLE COMPOSITE COVER FOR MISSILE LAUNCH TUBE. Master of Science Thesis, Middle East Technical University, **2018**

12. Zhou, G. et al., A new frangible composite canister cover with the function of specified direction separation, Applied Composite Materials, 23(4), pp. 623–638, **2016**

13. Chung, J.-W., Shin, S.-M. and Bae, Y.-G., Test Technique for Performance Verification of Fracture-Type Canister Cover, Journal of the Korea Institute of Military Science and Technology, 16, pp. 449–455, **2013**

14. Wu, J.H., Wang, W.T. and Kam, T.Y., Failure Analysis of a Frangible Laminated Composite Canister Cover, Proceedings of the Institution of Mechanical Engineers, Part G: Journal of Aerospace Engineering, 213(3), pp. 187–195, **1999**

15. S. P. Marsh, LASL Shock Hugoniot Data, University of California Press, ISBN 0-520-04007-4, **1980**

16. Walter, P.L., Air-Blast and the Science of Dynamic Pressure Measurements, Sound & Vibration, 38, pp. 10–17, **2004**

17. Model M102B15 high frequency ICP® pressure sensor, 200 PSI, 25 | PCB, Available at:

https://www.pcb.com/contentstore/docs/PCB_Corporate/Pressure/Products/Manuals/M102B15.pdf (Accessed: February 21, 2023).

18. Sutton, G.P. and Biblarz, O., Rocket Propulsion Elements. Hoboken, NJ: John Wiley & Sons, Inc., **2017**

19. CEARUN REV3C (no date) NASA. NASA. Available at: https://cearun.grc.nasa.gov/ (Accessed: February 26, 2023).

20. Fernandes, F. A. C., Souto, C. D., and Pirk, R., Static Firing Tests of Solid Propellant Rocket Motors: Uncertainty Levels of Thrust Measurements, Journal of Aerospace Technology and Management, 14, **2022**

21. Ma, Y., Jiang, Y., Hao, J., and Yan, F., Simulation of the Influence of Missile Exhaust Plume to the Launching Equipment, 2010 International Conference on Measuring Technology and Mechatronics Automation, ICMTMA 2010, 3, 370–373, **2010**

22. Nabulsi, A.A.L., Rigid Polyurethane Foam: Mechanistic Study and Catalyst Development. thesis. Doctoral Thesis., RWTH Aachen, **2018**

23. High pressure and low pressure dosing machine (2021) Cannon PlasTec. Available at: https://www.cannonplastec.com/products/machinery/dosing-machine/ (Accessed: February 26, 2023).

24. Ridha, M., Mechanical and Failure Properties of Rigid Polyurethane Foam Under Tension, Doctoral Thesis, National University of Singapore, **2007**

25. Widdle, R.D., Bajaj, A.K. and Davies, P., Measurement of the Poisson's ratio of flexible polyurethane foam and its influence on a uniaxial compression model, International Journal of Engineering Science, 46(1), pp. 31–49., **2007**

26. Ave 2 non-contacting video extensometer | instron. Available at: https://www.instron.com/en/products/testing-accessories/extensometers/non-contacting-video (Accessed: February 21, 2023).

27. Fracture mechanics (2023) Wikipedia. Wikimedia Foundation. Available at: https://en.wikipedia.org/wiki/Fracture_mechanics (Accessed: February 26, 2023).

28. Rao Lakshmana C., Narayanamurthy V., and Simha K. R. Y., Applied Impact Mechanics, Ane Books Pvt. Ltd. (ISBN : 978-11-1924-180-5), **2016**

29. Ansys Explicit Dynamics | ansys training. (Available at: https://www.ansys.com/training-center/course-catalog/structures/ansys-explicit-dynamics (Accessed: February 26, 2023).

30. R. Courant, K. Friedrichs and H. Lewy, On the Partial Difference Equations of Mathematical Physics, IBM Journal of Research and Development, Vol. 11, No. 2, pp. 215-234, **1967**

31. Herrmann, W., Constitutive Equation for the Dynamic Compaction of Ductile Porous Materials. Journal of Applied Physics, 40(6), **1969**

32. M. Carroll and A. C. Holt, Marsh, LASL Shock Hugoniot Ductile Porous Materials, J. Appl. Phys. Vol. 43, number 4, April, **1972**

33. Wardlaw, A., McKeown, R. and Chen, H., Implementation and Application of the P-alpha Equation of State in the DYSMAS Code, **1996**

34. Abaqus Analysis User's Guide (6.14) - 130.149.89.49:2080 (no date). Available at: http://130.149.89.49:2080/v6.14/books/usb/default.htm (Accessed: February 26, 2023).

35. Gibson, L., & Ashby, M., Cellular Solids: Structure and Properties (2nd ed., Cambridge Solid State Science Series), Cambridge: Cambridge University Press, doi:10.1017/CBO9781139878326, **1997**

36. D. E. Grady and N. A. Winfree, A Computational Model for Polyurethane Foam, In: Staudhamer KP, Murr LE and Meyers MA., editors, Fundamental Issues and Applications of Shock-Wave and High Strain-Rate Phenomena. Elservier-Science, 485-491, **2001**

37. Lloyd, A.N., The static and dynamic compaction characteristics of porous silica powder: An experimental and numerical approach, Master of Science Thesis, Faculty of the Graduate School, Marquette University, Milwaukee, Wisconsin, **2006**

38. M. Meyers, Dynamic Behavior of Materials. Wiley Press, **1994**

39. Laine, L. and Sandvik, A., 4th Asia-Pacific Conference on Shock and Impact Loads on Structures, Derivation of Mechanical Properties for Sand, pp. 361–368., **2001**

40. Merillas, B.; Villafañe, F.; Rodríguez-Pérez, M.Á. A New Methodology Based on Cell-Wall Hole Analysis for the Structure-Acoustic Absorption Correlation on Polyurethane Foams. Polymers, 14, 1807. https://doi.org/10.3390/polym14091807, **2022**

APPENDIX

APPENDIX 1 – Dynamic Pressure Sensor

Model Number	ICP® PRESSURE SENSOR		Revision: D
102B			ECN #: 53357

Performance	ENGLISH	SI	
Measurement Range(for ±5V output)	5,000 psi	34,500 kPa	
Useful Overrange(for ± 10V output)	10,000 psi	69,000 kPa	[1]
Sensitivity(± 10 %)	1.0 mV/psi	0.15 mV/kPa	
Maximum Pressure(static)	15,000 psi	103,000 kPa	
Resolution	20 mpsi	0.14 kPa	[2]
Resonant Frequency	≥ 500 kHz	≥ 500 kHz	
Rise Time(Reflected)	≤ 1.0 μ sec	≤ 1.0 μ sec	
Low Frequency Response(- 5 %)	0.001 Hz	0.001 Hz	
Non-Linearity	≤ 1.0 % FS	≤ 1.0 % FS	[3]
Environmental			
Acceleration Sensitivity	≤ 0.002 psi/g	≤ 0.0014 kPa/(m/s²)	
Temperature Range(Operating)	-100 to +275 °F	-73 to +135 °C	
Temperature Coefficient of Sensitivity	≤ 0.03 %/°F	≤ 0.054 %/°C	[2]
Maximum Flash Temperature	3,000 °F	1,650 °C	
Maximum Shock	20,000 g pk	196,000 m/s² pk	
Electrical			
Output Polarity(Positive Pressure)	Positive	Positive	
Discharge Time Constant(at room temp)	≥ 500 sec	≥ 500 sec	
Excitation Voltage	20 to 30 VDC	20 to 30 VDC	
Constant Current Excitation	2 to 20 mA	2 to 20 mA	
Output Impedance	≤ 100 Ohm	≤ 100 Ohm	
Output Bias Voltage	8 to 14 VDC	8 to 14 VDC	
Electrical Isolation	10⁸ Ohm	10⁸ Ohm	
Physical			
Sensing Geometry	Compression	Compression	
Sensing Element	Quartz	Quartz	
Housing Material	Stainless Steel	Stainless Steel	
Diaphragm	Invar	Invar	
Sealing	Welded Hermetic	Welded Hermetic	
Electrical Connector	10-32 Coaxial Jack	10-32 Coaxial Jack	
Weight	0.44 oz	12.5 gm	

OPTIONAL VERSIONS

Optional versions have identical specifications and accessories as listed for the standard model except where noted below. More than one option may be used.

CA - Ablative Coating

M - Metric Mount
Supplied Accessory: Model 065A40 Seal ring 0.435" OD x 0.397" ID x 0.030" thk brass (1) replaces Model 065A03

N - Negative Output Polarity

S - Stainless Steel Diaphragm
Diaphragm   316L Stainless Steel   316L Stainless Steel

W - Water Resistant Cable

NOTES:
[1] For +10 volt output, minimum 24 VDC supply voltage required. Negative 10 volt output may be limited by output bias.
[2] Typical.
[3] Zero-based, least-squares, straight line method.
[4] See PCB Declaration of Conformance PS023 for details.

SUPPLIED ACCESSORIES:
Model 065A03 Seal ring 0.435" OD x 0.377" ID x 0.030" thk brass (3)

Entered: ND	Engineer: RPF	Sales: RWM	Approved: RPF	Spec Number:
Date: 11/30/2022	Date: 11/30/2022	Date: 11/30/2022	Date: 11/30/2022	40708

PCB PIEZOTRONICS
AN AMPHENOL COMPANY
3425 Walden Avenue, Depew, NY 14043
Phone: 716-684-0001
Fax: 716-684-0987
E-Mail: info@pcb.com

CE [4]

All specifications are at room temperature unless otherwise specified.
In the interest of constant product improvement, we reserve the right to change specifications without notice.
ICP® is a registered trademark of PCB Piezotronics, Inc.

.

APPENDIX 2 – Pyroceram Code 9606

Corning® Pyroceram® glass-ceramic material is opaque, light gray in color, and has high strength, high elastic modulus, and uniform dielectric properties. It can be manufactured in ogival* shapes, hemispheres, pressware sheets, and various machined shapes.

* pointed arch

Applications

Tactical Missile Nosecones
Antenna Windows
Radomes
Solid Wave Guides
Hydrospace Systems

Dimensions

Ogival Shapes	Up to 48 inches long x 20 inches diameter
Hemispheres	Up to 16 inches in diameter
Pressware Sheets	Up to 27 inches x 27 inches x 1.0 inch or 17 inches x 17 inches x 2.0 inches

Physical Properties

Water Absorption	< 0.01%
Softening Point	1350 °C; 2462 °F
Gas Permeability	Impermeable
Density	2.6 g/cm³; 160 lb/ft³
Elastic Modulus	120 x 10⁶ kPa; 17.4 x 10⁶ psi

Thermal Properties

Coefficient of Linear Expansion	$57 \times 10^{-7}/°C - 32 \times 10^{-7}/°F$ (20 °C - 320 °C; 68 °F - 608 °F)
Thermal Conductivity	0.0081 cal/(s·cm·°C) — 2 BTU·ft/(h·ft²·°F) (mean 20 °C - 800 °C — 68 °F - 1472 °F)
Thermal Diffusivity	0.0127 cm²/s — 0.049 ft²/h (mean 20 °C - 800 °C — 68 °F - 1472 °F)
Specific Heat	0.233 cal/(g·K) — 0.233 BTU/(lb·°F) (mean 20 °C - 800 °C — 68 °F - 1472 °F)

For more information about Corning's Pyroceram® materials please contact:

CORNING

.